Title

Transcriptional regulation of N6-methyladenosine orchestrates sex-dimorphic metabolic traits

Journal

Nature Metabolism, 3(7)

ISSN

2522-5812

Authors

Salisbury, David A
Casero, David
Zhang, Zhengyi
et al.

Publication Date

2021-07-01

DOI

10.1038/s42255-021-00427-2

Peer reviewed

HHS Public Access

Author manuscript

Nat Metab. Author manuscript; available in PMC 2022 January 19.

Published in final edited form as:

Nat Metab. 2021 July ; 3(7): 940–953. doi:10.1038/s42255-021-00427-2.

Transcriptional regulation of *N*^{6}-methyladenosine orchestrates sex-dimorphic metabolic traits

David A. Salisbury[1,2,3], **David Casero**[4], **Zhengyi Zhang**[1,2], **Dan Wang**[1,2], **Jason Kim**[1,2], **Xiaohui Wu**[1,2], **Laurent Vergnes**[5], **Aashiq H. Mirza**[6], **Paola Leon-Mimila**[1,7], **Kevin J. Williams**[8], **Adriana Huertas-Vazquez**[1], **Samie R. Jaffrey**[6], **Karen Reue**[2,5], **Jianjun Chen**[9], **Tamer Sallam**[1,2,3,*]

[1] Division of Cardiology, Department of Medicine, University of California, Los Angeles, CA

[2] Molecular Biology Institute, University of California, Los Angeles, CA

[3] Molecular Biology Interdepartmental Program, University of California, Los Angeles, CA

[4] F. Widjaja Foundation Inflammatory Bowel & Immunobiology Research Institute, Cedars-Sinai Medical Center, Los Angeles, CA

[5] Department of Human Genetics, University of California, Los Angeles, CA

[6] Department of Pharmacology, Weill Cornell Medicine, Cornell University, New York, NY

[7] Unidad de Genómica de Poblaciones Aplicada a la Salud, Facultad de Química, Universidad Nacional Autónoma de México, Mexico City, Mexico.

[8] Department of Biological Chemistry, University of California, Los Angeles, CA

[9] Department of Systems Biology, The Beckman Research Institute of City of Hope, Duarte, CA

Abstract

Males and females exhibit striking differences in the prevalence of metabolic traits including hepatic steatosis, a key driver of cardiometabolic morbidity and mortality. RNA methylation is a widespread regulatory mechanism of transcript turnover. Here, we show that presence of the RNA modification N^6-methyladenosine (m6A) triages lipogenic transcripts for degradation and guards

*Corresponding author, Contact Information: Division of Cardiology, Department of Medicine, David Geffen School of Medicine at UCLA, 650 Charles E. Young South Dr. CHS A2-327, Los Angeles, CA 90095-1679, tsallam@mednet.ucla.edu.

Author contributions:

TS conceived and supervised the study. TS and DS designed the study, guided the interpretation of the results and preparation of the manuscription. DS, XW, JK, DW performed the majority of experiments and data analysis. ZZ performed the ATAC-seq experiments and data analysis. LV and KR performed the fatty acid oxidation studies and studies determine the influence of chromosomal versus gonadal factors in Mettl14 regulation and guided the interpretation of results. KJW performed lipidomics studies and analysis. AM and SJ performed m^{6}A measurement via mass spectrometry. AHV analyzed the data for MBBS. JC assisted with m^{6}A loss of function *in vivo* studies and cellular knockdown. DC performed m^{6}A and RNA-seq analysis. TS wrote the manuscript with input from all authors. All authors discussed the results and approved the final version of the manuscript.

Competing Interests:

J.C. is a scientific founder of Genovel Biotech Corp. and holds equities with the company, and is also a Scientific Advisor for Race Oncology. A patent related to this work is issued to T.S. The other authors declare no competing conflict of interest.

Datasets Availability:

RNA-seq, m^{6}A-seq, and ATAC-seq data can be accessed under NIH's SRA repository PRJNA663718 and GSE157907.

against hepatic triglyceride accumulation. In male but not female mice, this protective checkpoint stalls under lipid-rich conditions. Loss of m6A control in male livers increases hepatic triglyceride stores leading to a more “feminized” hepatic lipid composition. Crucially, liver-specific deletion of the m6A complex protein Mettl14 from male and female mice significantly diminishes sex-specific differences in steatosis. We further surmise that m6A installing machinery is subject to transcriptional control by the sex-responsive BCL6-STAT5 axis in response to dietary conditions. These data show that m6A is essential for precise and synchronized control of lipogenic enzyme activity and provide insights into the molecular basis for the existence of sex-specific differences in hepatic lipid traits

The liver is the central tissue orchestrating rapid adaptations in gene regulation to maintain metabolic homeostasis. Control of mRNA biogenesis is a key target of multiple regulatory pathways in liver and its disruption can result in metabolic disturbances including fatty liver disease. For example, chronic high fat/high carbohydrate feeding stimulates the master lipogenic transcription factor SREBP1C, transcriptional induction of lipogenic genes, and increased hepatic triglyceride stores [1]. Reciprocally, under fasting conditions, activity of SREBP1C and its downstream targets *Scd1*, *Dgat2* and *Fasn* are reduced [1,2]. Fasting is characterized by low insulin, almost absent nuclear SREBP1C and low demand for fatty acid biosynthesis[3]. Mysteriously, despite lower level of lipogenic mRNA and protein compared with fed state in liver, the absolute expression of lipogenic genes during fast is remarkably high (top 0.1–2% by percentile rank). Others have reported sex-specific discordance in lipogenic mRNAs, their protein levels and/or triglyceride content [4,5]. These observations hint the existence of a post-transcriptional axis contributing to lipogenesis; however, the mechanisms underlying synchronized control of lipogenic mRNA metabolism and protein function remain poorly understood.

Recent evidence suggests that selective N^6-methyladenosine (m^6A) methylation of RNA can affect the stability, translation and/or localization of mRNA[6–8]. The installation of m^6A occurs at predictable motifs through the collaborative activities of a ‘writer ‘ complex made up of the methyltransferases METTL14 and METTL3 [9]. Although a group of elegant studies have shown that m^6A plays a critical role in diverse biologic processes [7,8,10], understating the molecular basis of temporospatial variation in m^6A levels and how the activity of m^6A installing machinery may be fine-tuned in response to environmental cues is still emerging. Here, we demonstrate that m^6A modifications potently alter the fate of lipogenic mRNA and hepatic triglyceride stores. In addition, we show that m^6A modifications are dynamically altered in response to dietary conditions and provide mechanistic evidence that m^6A installing machinery is subject to tight transcriptional control by sex-dimorphic dietary regulators to sustain metabolic control. These data identify a new pathway for lipid degradation and, at least in part, explain the molecular basis for the existence sex-specific differences in hepatic triglyceride composition.

Results

RNA methylation strongly enriches lipogenic transcripts and is dynamically regulated with diet

Chemical modifications on RNA are critical for the ability of cells to execute development programs and to respond to environmental challenges. To further investigate the contributions of RNA modifications in metabolic control, we performed unbiased interrogation of mRNA, lipids, and RNA methylation patterns using m^{6}A-seq [8] on livers from mice (C57BL/6) fed chow, western diet (WD) or high fat (HF) diet (Fig. 1a). As expected, HF or WD feeding led to increased weight gain, fat composition, and serum lipids at 2 weeks or 4 weeks (Extended Data Fig. 1a–i). Principal component analysis (PCA) of genome-wide RNA abundances segregates sample groups, showing that sex is the dominant factor influencing gene expression and diet composition playing a critical, but secondary role (Fig. 1b). Length of diet feeding did not a have a strong impact on gene expression. Congruently, PCA of unbiased lipidomics showed a similar trend, with sex and diet being the strongest variables influencing hepatic lipid composition (Extended Data Fig. 2a). We observed minimal shifts in most lipid species across groups (Extended Data Fig. 2b–d), but striking differences were noted for a number of neutral lipids including triglycerides (Fig. 1c). In line with PCA results, sex had a strong influence on fasting triglyceride content irrespective of diet composition with females consistently having higher levels than males (Fig. 1c).

Examination of the RNA methylation landscape in liver showed the m^{6}A modifications strongly clustered near 3’ UTR regions or last exons in line with previous reports (Fig. 1d) [11,12]. In addition, we find that the RNA methylome is enriched at consensus motifs known to be bound by the METTL3/METTL14 complex (Fig. 1d) [12]. Intriguingly, PCA analysis based on global m^{6}A patterns led to stronger segregation of samples than use of gene expression alone (Fig. 1e and Extended Data Fig. 2e). We examined dynamic changes in m^{6}A profiles with dietary conditions using several unbiased approaches, including comparing fold enrichment of m^{6}A with diet as well as examining the contributions of individual genes to variance. Regardless of approach, consistent enrichment of lipogenic genes was observed. PCA analysis showed that *Scd1* had multiple m^{6}A peaks that were in the top 20 most significant peaks contributing to variance of over 10,000 m^{6}A peaks detected (#4 and #14). Western diet (WD) feeding led to a reduction in the number of hypermethylated peaks (Fig. 1f). Comparison of chow and WD showed that differentially regulated m^{6}A peaks preferentially enriched lipogenic pathways with many lipogenic genes containing m^{6}A consensus motifs (Fig. 1g–h and Extended Data Fig. 2f–g). In agreement with these findings, m^{6}A profiles were reduced on lipogenic transcripts during WD feeding in comparison with chow (Fig. 1h). We confirmed our findings using m^{6}A-IP-RT-qPCR (Fig. 1h). A similar pattern was observed when comparing HF versus chow, where HF feeding led to a reduction in m^{6}A on mRNAs involved in fatty acid and triglyceride biosynthesis (Fig. 1h and Extended Data Fig. 2h). Taken together, our data suggest that m^{6}A peaks are strongly enriched on lipogenic mRNAs in liver and that their deposition is highly sensitive to dietary conditions.

Liver-specific deletion of the m^{6}A methylase METTL14 increases lipogenesis.

The RNA modification m^{6}A is installed by a multiprotein complex containing METTL3 and METTL14 [6,13]. Disruptions of the catalytic enzyme METTL3 or its allosteric activator METTL14 disrupts m^{6}A modifications on target RNAs [13,14]. To directly investigate the contributions of m^{6}A in hepatic lipid metabolism, we generated mice with liver-specific deletion of *Mettl14* (referred to as L-KO) by administering AAV8.tbg.cre [15,16] or AAV8.tbg.control (referred to as control or WT for paired experiments) to *Mettl14*$^{flox/flox}$ mice. We confirmed that METTL14 is readily deleted in liver but not in other tissues after 4 weeks on chow diet (Fig. 2a and Extended Data Fig. 3a). Unbiased lipidomics showed a dramatic increase in triglyceride content in *Mettl14* L-KO livers compared with controls (Fig. 2b). The vast majority of other lipid classes were unchanged comparing WT or *Mettl14* L-KO (Fig. 2b and Extended Data Fig. 3b–c).

We did not observe changes in food intake or body weight including fat mass in the setting of loss of METTL14, suggesting that altered caloric balance is not a contributor to triglyceride accumulation (Extended Data Fig. 3d–e). Since changes in hepatic fatty acid oxidation can reciprocally affect triglyceride stores, we measured mitochondrial fatty acid metabolism in whole liver. Our results showed no change fatty acid oxidation in *Mettl14* L-KO livers compared with controls (Extended Data Fig. 3f). Measurement of genes involved in B oxidation showed no change or slight increase, suggesting that the observed increase in hepatic triglyceride stores cannot be explained by changes in beta oxidation or altered mitochondrial function (Extended Data Fig. 3g). Similarly, serum triglycerides, hepatic *Apob*, lipid export and lipolysis genes were minimally altered suggesting that impaired lipid secretion or lipid droplet breakdown is not a cause of triglyceride accumulation (Extended Data Fig. 3h–i).

Given that m^{6}A modifications are known to predominantly affect gene regulation by impacting mRNA stability, which can then result in corresponding changes in translation [8–10,17,18], we measured protein levels of major lipogenic genes. We observed a significant increase in protein levels of lipogenic genes in *Mettl14* L-KO compared with controls (Fig. 2c and Extended Data Fig. 3j). We confirmed this critical finding in *Mettl14* L-KO generated using crosses with *Cre*^{Alb} transgenics, suggesting that the effects of hepatic *Mettl14* deletion are sustained in both acute and chronic perturbations (Extended Data Fig. 3k–l). Taken together, these results suggest that enhanced fatty acid and triglyceride biosynthesis are the major contributors to triglyceride accumulation in *Mettl14* L-KO. Notably, we observe an increase in polyunsaturated fatty acids and SCD1 index or “desaturation index” in *Mettl14* L-KO in line with the observed increase in fatty acid biosynthetic enzymes (Fig. 2d) [19]. Protein levels and gene expression of other genes involved in triglyceride metabolism such as *Apoe*, *Apob*, *Mttp* were not increased (Extended Data Fig. 3i–j). In addition, we confirmed reduced m^{6}A enrichment of lipogenic transcripts in *Mettl14* L-KO using m^{6}A-IP-RT-qPCR (Extended Data Fig. 3m–n). Collectively, our findings are consistent with idea that RNA modification act to repress lipogenic proteins in the liver and are congruous with the observed changes in m^{6}A landscape in response to diet.

It is well established that SREBP signaling is the dominant mechanism that influences lipogenic gene transcription and feedback regulation [1,20]. To more thoroughly investigate

how m^{6}A modifications affect *Srebp1c* and lipogenesis, we measured mRNA levels of fatty acid biosynthetic genes. Despite the observed increase in lipogenic proteins and triglycerides levels, lipogenic mRNAs and pre-mRNA were reduced (Extended Data Fig. 4a–b). These results are in line with multiple previous studies showing that accumulation of polyunsaturated fatty acids (PUFAs) suppresses SREBP1C processing and potently feeds back on lipogenic gene transcription [1,21]. In addition, we found that loss of *Mettl14* L-KO led to a marked reduction in *Srebp1c* mRNA and nuclear SREBP1C protein (Extended Data Fig. 4a–c). Measurement of gene expression at an earlier timepoint (72 hours versus 4 weeks), where PUFA accumulation is reduced, showed an increase in lipogenic mRNAs (Extended Data Fig. 4d). Taken together, these results imply that the discordance between RNA and protein levels may be a late effect due to rampant accumulation of PUFAs. More importantly, the data suggests that a primary perturbation in fatty acid biosynthetic gene transcription is unlikely to explain the observed phenotype. We therefore reasoned that altered mRNA stability and/or protein translation may be at play, consistent with known roles of m^{6}A. To explore this further, we performed ribosome profiling from control or *Mettl14* L-KO livers which showed that loss of METTL14 enhances the abundance of lipogenic mRNAs but not all transcripts in the translating pool compared with controls (Fig. 2e and Extended Data Fig. 4e–f). To test whether METTL14 regulates lipogenic genes through modulating their mRNA stability, we performed mRNA stability assays using the transcription inhibitor actinomycin D in primary hepatocytes isolated from control and *Mettl14* L-KO (Fig. 2f–g, Extended Data Fig. 4g, Equation 1–2). In the setting of transcriptional inhibition, we observed enhanced mRNA stability of lipogenic mRNAs in *Mettl14-KO* versus control hepatocytes (Fig. 2f–g and Extended Data Fig. 4g). Taken together, these results imply that increased protein levels of lipogenic genes is due to enhanced mRNA stability and downstream translation, in agreement with other evidence that internal RNA modifications impact mRNA dynamics to alter protein levels [6–8]. Complementing these results, we observed increased *Scd1* mRNA abundance in the setting of loss of *Mettl14* by fluorescence in situ hybridization (FISH) (Fig. 2h and Extended Data Fig. 4h). Interestingly, knockdown of *Mettl14* decreased localization of *Scd1* with DCP1a, a key decapping enzyme involved in mRNA degradation pathways and a marker of processing bodies (Fig. 2h). To reinforce the idea that post-transcriptional mechanisms are more critical factors in the effects of m^{6}A, we observed that knockdown of *Mettl14* enhances mRNA levels of lipogenic transcripts in setting of functional SREBP deficiency (*Scap*$^{-/-}$) [22,23] (Fig. 2i). Collectively, our findings suggest that increased biosynthesis of lipogenic mRNAs does not contribute to the observed increase in fatty acid and triglyceride levels in *Mettl14* L-KO and that post-transcriptional mechanisms are more critical drivers of the observed change in hepatic lipid composition.

METTL14 expression is inversely correlated with human fatty liver disease

To investigate the potential contribution of m^{6}A in human fatty liver disease, we examined the expression of *METTL14* in liver from the Mexican Obesity Surgery (MOBES) cohort which includes non-related Mexican Mestizo patients aged 18–59 [24]. Unique strengths of this study include using a gold-standard liver biopsy to confirm the presence and grading of NAFLD by Kleiner's scoring method[25]. Patients were classified in 3 groups: controls (normal histology), simple steatosis (steatosis grade ranging from 1 to 2), and NASH (NAS>

5) based on independent scores from two experience pathologists. Clinical, metabolic and biochemical data were collected from all participants. *METTL14* expression was negatively correlated with human steatosis and NASH (Fig. 3a–b). Although triglyceride content is one of many factors that determine progression to chronic liver disease, these findings are consistent with our observed animal studies and hint at functional conservation of our proposed mechanisms.

Our results hint that modulation of m^{6}A levels can influence pathologic fat storage in liver, which led to tested an m^{6}A-based gene therapy strategy overexpressing the METTL3/METTL14/WTAP 'writer' complex in a mouse model of nonalcoholic fatty liver disease (NAFLD) (Fig. 3c). *In vivo* administration of m^{6}A writers using an AAV8 with a liver-specific promoter enhanced gene expression of MTA complex components (Fig. 3d) and m^{6}A enrichment on lipogenic mRNA (Fig 3e). In addition, m^{6}A writers overexpression reduced lipogenic proteins (Fig. 3f) and resulted in modest decrease in Oil-red-O staining, and hepatic triglyceride content although results did not reach significance (Fig. 3g and Extended Data Fig. 4i). We observed a significant reduction in genes associated with inflammation and fibrosis (Fig. 4h), key drivers of NASH progression. It should be noted that chronic overexpression of METTL14 alone was not sufficient to alter lipogenic proteins (not shown) probably since its catalytic partner METTL3 is required to efficiently enhance m^{6}A deposition. Recent evidence suggests that site-specific programmable RNA modification is readily achievable with minimal off target effects using a guide RNA and a dCas13-tethered writer complex [14,26,27]. To test the influence of programmable RNA methylation of lipogenesis, we introduced an RNA methylation modifying complex with individual RNA guides targeting *Scd1* m^{6}A sites (Fig. 3i). Targeted RNA methylation enhanced *Scd1* m^{6}A levels measured by m^{6}A-IP-RT-qPCR and resulted in lower protein levels of SCD1 (Fig. 3j–k). Altogether, our findings hint at strong relevance of m^{6}A in regulation of human fatty liver and that modulation of RNA methylation through multiple approaches, including an FDA approved platform, is technically feasible and efficacious in reducing important markers of chronic liver disease.

m^{6}A machinery undergoes transcriptional regulation by sex-biased transcription factors

Our global methylome analysis revealed a reduction in m^{6}A signatures with WD or HF feeding in male mice along with a potent decrease in lipogenic RNA modification (Fig. 1). In line with these results, we find that chronic WD feeding resulted in a significant increase in hepatic triglycerides in male *Mettl14* L-KO compared to controls (Fig. 4a–b), but the effect size was diminished in comparison with chow diet (Fig. 4a and Fig. 2b). Similarly, loss of *Mettl14* resulted in only a mild increase in lipogenic enzymes under WD as opposed to the dramatic effect observed under chow conditions (Fig. 4c). Consistent with chow feeding results, we did not observe major changes in other lipid species (Extended Data Fig. 5a). Interestingly, the fed state was associated with a reduction in METTL14 protein and loss of *Mettl14* resulted in no observable change in triglycerides or lipogenic proteins under refed conditions, when lipogenesis is known to be highest (Fig. 4d–e). These findings imply that m^{6}A modifications appear to be more relevant under basal fasting conditions where there is minimal demand for *de novo* fatty acid biosynthetic enzymes and that contributions of m^{6}A are diminished under western diet or refeed conditions. Thus, m^{6}A modifications

act in coordinate fashion with transcriptional control mechanisms driven by SREBP1C, becoming less important when SREBP1C driven lipogenesis is at play.

To better explore the mechanism of reduction in m^{6}A with dietary challenge, we investigated the regulation of *Mettl14*. In line with the findings in Fig. 4c, we observed a decrease in the expression of the m^{6}A writer *Mettl14* with either HF or WD (Fig. 4f). We confirmed that METTL14 protein is reduced with diet feeding (Fig. 4g). Intriguingly, the pattern of regulation in male mice was the opposite of what we observed in female mice where WD or HF feeding did not reduce *Mettl14* mRNA and protein levels and in fact trended to increase (Fig. 4f–g). We measured m^{6}A levels in liver using mass spectrometry which closely mirrored the *Mettl14* regulation pattern (Fig. 4h). To further explore the basis of the sex-specific differences in *Mettl14,* we used a genetic model that segregates gonadal sex from chromosomal sex effects by generating XX and XY mice with ovaries, and XX and XY mice with testes on a hyperlipidemic background [28]. We found that XX animals have higher *Mettl14* levels than XY (Fig. 5a), consistent with the observed regulation of *Mettl14* under lipid-rich conditions (Fig. 4f–g). These results imply that *Mettl14* levels are strongly influenced by chromosomal sex composition. In addition, examination of publicly available histone marks in liver under different dietary conditions led us to hypothesize that *Mettl14* may be subject to tight transcriptional regulation, since H3K27ac, a mark of transcriptional activation, was reduced with high fat feeding (Extended Data Fig. 5b). To more thoroughly explore the molecular basis of alteration in METTL14 and m^{6}A with diet feeding, we performed ATAC-seq in liver under chow, WD or HF (Fig. 5b). This technique tags accessible genome sites with sequencing adaptors to provide a multidimensional view of gene regulation [29]. We did not observe dramatic changes in accessibility or chromatin rearrangements in response to diet feeding at the *Mettl14* locus (Fig. 5b). We noted, however, a single open access site was which we reasoned may be critical for docking of canonical regulatory factors or recruiting additional factors with dietary perturbations within this region. Motif interrogation of accessible regions revealed binding of a number of factors known to be involved in metabolic control including the sexually-dimorphic STAT5A and BCL6 complex[30–32]. ChIP-seq studies confirmed the binding of STAT5a and BCL6 at *METTL14* in both mice and humans (Extended Data Fig. 5c–d). Consistent with previous studies [30,31], we observed an increase in *Bcl6* levels with diet and feeding state (Fig. 5c and Extended Data Fig. 5e). Levels of m^{6}A on lipogenic transcripts were altered comparing fast and refed state (Extended Data Fig. 5f). In addition, other MTA complex proteins were also differentially regulated with diet composition or feeding state (Extended Data Fig. 5g–h). Interestingly, binding of BCL6 has been shown to repress STAT5 targets in male but not female livers [33,34]. In addition, hepatic loss of *Bcl6* has been shown to have the opposite phenotype of the *Mettl14* L-KO where it reduces triglyceride stores [30]. These results hint that the observed reduction in *Mettl14* enzyme levels in male but not female mice with dietary challenge may be mediated by BCL6 repressive effects at the *Mettl14* promoter region. To directly test this theory, we generated *Bcl6* liver-specific knockout mice (*L-Bcl6*$^{-/-}$). When fed WD, *L-Bcl6*$^{-/-}$ mice showed no differences in *Mettl14* mRNA and protein levels between the sexes in stark contrast to the differences observed in WT mice (Fig. 5d–e). Overall, these results strongly suggest the existence of sex-specific differences

in RNA methylation and that m^{6}A installing machinery is subject to tight transcriptional control.

Loss of m^{6}A diminishes sex-specific differences in hepatic lipid composition and sex-biased gene expression.

Multiple studies reported on sex-specific differences in lipogenic mRNAs, their protein abundance as well as fatty liver traits across species, albeit the direction of these differences varied depending on species, genetic background, and context [5,35–37]. Female mice were noted to have higher fasting liver triglyceride than males but not necessarily all lipid species [5,36], which is in line with our findings (Fig. 6a). Transcriptome-wide gene expression analysis showed minimal differences in lipogenic mRNAs between the sexes regardless of diet (Fig. 6b). We confirmed by RT-qPCR that differences in lipogenic RNAs do not explain the observed sex-differences in fasting hepatic triglyceride content (Fig. 6c), although surprisingly females were noted to have markedly higher protein level of fatty acid and triglyceride synthesis enzymes compared with males (Fig. 6d). *Scd1,* for example, showed higher RNA levels in males despite having higher protein levels in females (Fig. 6c–d). A similar trend was observed for other genes involved in triglyceride biosynthesis where strikingly higher protein levels were noted in females despite minimal differences in gene expression. These results imply that post-transcriptional mechanisms may be contributing to sex-specific variation in lipogenic proteins and triglyceride content. Remarkably, the protein levels of lipogenic genes were discordant with sex-differences in m^{6}A where males had higher m^{6}A levels than females on lipogenic mRNAs (Fig. 6e). These findings are in line with the above results (Fig. 2 and Fig. 3) and reinforce the idea that m^{6}A modifications on lipogenic transcripts may be a factor contributing to sex-differences in lipogenic protein levels and triglyceride content. To test this hypothesis more directly, we compared the effect of *Mettl14* deletion between the sexes and found that liver-specific deletion of *Mettl14* diminished the striking differences in lipogenic protein levels between male and female mice (Fig. 6f). In addition, we note that under chow conditions liver-specific deletion of *Mettl14* in male mice increased triglyceride levels, almost matching WT female mice, suggesting that m^{6}A activity leads to suppression of triglyceride levels and its loss leads to a more “feminized” lipid composition (Fig. 6g). Loss of m^{6}A control in females under chow conditions led to only a modest increase in triglyceride content (Fig. 6g). Reciprocally, loss of *Mettl14* in female mice was associated with greater differences in hepatic triglyceride compared with males under WD conditions (Fig. 6g). These results are consistent with the sex-dimorphic regulation of *Mettl14* (Fig. 5). Taken together, our findings strongly imply that sex-differences in fasting triglyceride stores are predominantly dictated by differences in RNA modifications.

To more thoroughly dissect the contributions of m^{6}A in hepatic sex-specific traits we performed RNA-seq on control and *Mettl14* L-KO male and female liver. PCA analysis of genome-wide mRNA abundances showed clear segregation between groups, with m^{6}A unexpectedly contributing to more variability in global RNA levels than sex (Fig. 6h). Remarkably, loss of *Mettl14* abolished m^{6}A-based differences in variance and significantly minimized sex-driven PCA variance, suggesting a strong interaction between RNA-modifications and sex-biased gene regulation (Fig. 6h). Notably, fitting the RNA-Seq

data to various multivariate additive and interaction models showed that the interaction between sex and *Mettl14* was significant for most sex-biased genes. This interaction resulted in a major reduction in sex-biased gene expression in *L-Mettl14* KO mice (Extended Data Fig. 6a–c) and hierarchical clustering revealed that L-*Mettl14* KO male mice consistently clustered with female samples (Extended Data Fig. 6c). Notably we did not observe differences in key regulators of sex-biased gene expression such as *Xist* and *Sry* (Extended Data Fig. 6d) and majority of the differentially regulated gene are not known to be direct targets of *Xist*. We used model-based clustering of all sex-biased and *Mettl14*-dependent genes to more rigorously evaluate the influence of sex on loss of m^{6}A. Consistent with our global analysis, a number of clusters showed dramatic abrogation of sex-biased gene expression in setting of loss of *Mettl14* (Extended Data Fig. 6e). Many of the genes in these clusters have been reported to define differences between male and female livers [38]. In addition, unsupervised interrogation of genes in these clusters revealed that multiple metabolic processes are the most enriched pathways under the interaction between m^{6}A and sex (Fig. 6i). In summary, our findings suggest that hepatic m^{6}A levels are important contributors to sex-biased gene expression and sex-specific lipid traits.

Discussion

In this work, we find that lipogenic mRNAs undergo chemical modifications that powerfully impact transcript turnover, adding another layer of dynamic gene regulation in hepatic lipid metabolism. The transcription factor SREBP1C, which is reduced during fasting and is activated by insulin and the lipid-responsive nuclear receptor Liver-X-receptor (LXR), play key roles in the induction of lipogenic genes through direct binding to lipogenic promoters [1,39]. Our model fits well with classical transcriptional mechanisms controlling lipogenesis and suggests that m^{6}A fine-tunes transcriptional outputs by enhancing mRNA degradation under conditions where hepatic fatty acid biogenesis may be in low demand.

A number of studies including our own have reported that female mice have higher basal fasting triglyceride levels than males but the molecular basis for these observations have been unknown [5,35–37]. We observed significant differences in the effects of m^{6}A between male and female mice and a strong influence of m^{6}A on the interaction between sex and diet composition. In male mice, loss of m^{6}A robustly impacted fatty acid biosynthesis and increased triglyceride stores under fasting chow conditions but its influence was diminished during western diet feeding, consistent with the observed decrease in m^{6}A. An opposite pattern was observed in female mice. Our findings here fill important gaps into the mysterious sex-specific differences in lipid composition but also suggest that there must be other factors beyond m^{6}A control that govern sex-differences in lipid composition. Although sex-differences in lipogenesis and triglyceride stores were dramatically diminished with loss of m^{6}A, it is important to point out that they were not entirely abrogated. Additionally, control of lipogenesis is one of many factors that influences hepatic lipid stores and it is likely that sex-differences related to other pathways such as mitochondrial bioenergetics, nuclear receptor outputs, or lipid uptake may be important. Finally, our study examined gene function during short-term dietary perturbations to more directly underpin mechanistic effects of m^{6}A. Although the influence of hepatic RNA modifications during prolonged feeding mimicking fatty liver disease is not well-defined, we predict, based on our findings,

that the female sex might confer a fitness advantage in chronic liver disease models. Despite starting with higher basal liver triglycerides, our data suggests that females are able to robustly leverage the protective effects of m^{6}A in the face of a dietary challenge whereas this unique lipid degradation pathways stalls in male mice under the same conditions. Congruent with this interpretation, we find that most human studies examining long-term dietary exposure showed higher risk of fatty liver disease in males compared with females [40]. We note, however, that disentangling the influence of covariates such as feeding state, diet composition, obesity, diabetes and alcohol consumption can be a challenge in population studies.

Contributions of m^{6}A seem to be more critical when SREBP1C driven lipogenesis is not in play, so at higher levels of gene transcription, the differential mRNA methylation is less important. Our findings add to other evidence suggesting that m^{6}A installation is actively regulated *in vivo* during health and disease states and impacts global m^{6}A levels [13]. Notwithstanding the known limitations in detecting changes using m^{6}A -seq [41], a strength of our study is using multiple complimentary approaches including knockout models to validate our main findings. However, we acknowledge that a major predicament in the field is understanding how changes in m^{6}A writers or erasers inform local or global changes in RNA methylation and it is possible that active regulation of m^{6}A machinery may not be the only mechanism specifying differences in lipid composition under different conditions. Indeed, our data hints that there may be ancillary variables that drive sensitivity to m^{6}A effects between the sexes. It is conceivable, for example, that a marked increase in lipogenic transcript biogenesis, which occurs during refeed, could overwhelm the enzymatic capacity of the methyltransferase complex which would render m^{6}A effects less meaningful during refeed. Thus, it is very likely that changes in stoichiometry critically dictate m^{6}A effects. We note that m^{6}A-seq cannot reveal the precise fraction of transcript copies modified by m^{6}A. In addition, measuring global m^{6}A in liver may not accurately reflect alterations in hepatocytes owing to diversity of other cell types in liver. Consistent with previous studies, our work suggests that m^{6}A installation reduces mRNA stability, an effect that does not require a functional SREBP axis. However, examination of RNA levels in liver after in chronic loss of function studies shows that lipogenic mRNAs are dramatically reduced in *L-Mettl14 KO* despite an increase in protein. This effect is likely due to PUFA accumulation since transcriptional feedback circuits are unchecked in *L-Mettl14 KO*. Indeed, a number of studies have shown that massive PUFA accumulation can result in half-life differences between RNA and protein levels [42,43].

We identify the BCL6-STAT5A axis as a critical regulator of *Mettl14* and m^{6}A content in the liver but it conceivable that other m^{6}A ‘writers’, ‘erasers’ or ‘readers’ may undergo similar dynamic regulation by the same axis or perhaps other relevant transcription factors. It is also possible that *Mettl14* may undergo additional post-translational processing. Intriguingly, deletion of *Bcl6* ameliorates hepatic steatosis [30] consistent with our findings that activation of *Bcl6* inhibits m^{6}A dependent degradation of transcripts that encode regulators of lipid synthesis. Finally, although our work focused on the role of m^{6}A in lipogenesis, it is important to point out that m^{6}A may have other contributions in metabolism. Future studies will investigate these questions more thoroughly.

Materials and Methods:

Reagents, plasmids, and cell transfection

shRNAs targeting *Mettl14* were obtained from Horizon Discovery and cloned into pLKO.1 vector (human:TRCN0000015935, mouse: TRCN0000084995). The resulting plasmids were transiently transfected using Fugene HD transfection reagent (Promega) or electroporated using the Neon transfection system (Invitrogen) and then tested for their ability to knockdown *Mettl14* at 48 hrs. AAV.TBG.PI.Cre.rBG (Addgene) was used for acute deletion of *Mettl14* and *BCL6* in mouse liver, AAV.TBG.PI.eGFP.WPRE.bGH (Addgene) or AAV.TBG.PI.Null.bGH (Addgene) were used as controls. For overexpression of m^6A writers, the following viruses were generated by VectorBuilder: AAV.TBG.mMettl3.WPRE, AAV.TBG.mMettl14.WPRE, and AAV.TBG.mWtap.WPRE. and AAV.TBG.PI.Null.bGH (Addgene) was used as the control. For targeted m^6A-modification of cellular mRNAs, plasmids encoding nuclease-dead *Cas13b* and truncated *Mettl3* fused to a nuclear localization sequence (pCMV-dCas13-M3nls) and gRNA expression plasmid (pU6-PspCas13b-gRNA) were obtained from Addgene (155366 and 155368). A complete list of antibodies and primers is available in Supplementary Tables 1 and 2.

Animals and diets

All animals used in this study were in C57BL/6 background unless otherwise noted. Our study used both male and female mice. Mice were housed in a temperature-controlled room under a 12-h light/12-hr dark cycle and pathogen-free conditions. Mice were fed standard chow diet, Western diet (40% Kcal with 0.15% cholesterol and moderate sucrose, or high fat diet (60%Kcal with moderate sucrose and no cholesterol) (Research Diets). Duration of diet was 4 weeks for most experiments but for male and female comparison WD RNA-seq experiments duration was shorter for 10 days. For m^6A writer overexpression experiments, mice were fed FPC-NASH diet (Envigo) and provided water supplemented with glucose and fructose (23.1g Fructose + 18.9g glucose in 1 L water, Sigma) for 8 weeks [44]. For RNA-seq, m^6A-seq, and m^6A writer *in vivo* overexpression experiments, age-matched WT mice were purchased from Jackson laboratories. *Mettl14*$^{f/f}$ mice were generated as previously described [13]. Age-matched male and female *bcl6* $^{f/f}$ mice and Albumin-cre transgenics were purchased from Jackson Laboratories. To generate liver-specific knockout mice, we treated *Mettl14*$^{f/f}$ and *bcl6* $^{f/f}$ mice with adeno-associated virus with TBG promoter (AAV8.TBG.Cre) or control (AAV8.TBG.GFP or AAV8.TBG.Null) purchased from Penn Vector Core. AAV was administered via intraperitoneal injection at a dose of 5×10^{11} GC per mouse. Four Core Genotypes (FCG) C57BL/6J mice on *Apoe* null background were from a colony maintained at UCLA. XX female mice were mated with XY–(Sry+) male mice to generate XX, XX(Sry+), XY–, and XY– (Sry+) [28]. To generate mice overexpressing m^6A writers in the liver, we treated 12 weeks old male mice purchased from Jackson Laboratories with 2.5×10^{11} GC each of AAV.TBG.mMettl3, AAV.TBG.mMettl14, and AAV.TBG.mWtap or 7.5×10^{11} GC of AAV8.TBG.Null per mouse. NAFLD diet composed of WD supplemented with glucose/fructose water. Mice were fasted for 4–6 hr prior to euthanization unless otherwise noted. All mouse experiments were approved by the UCLA institutional Animal Care and Research Advisory Committee.

Cell culture

Mouse primary hepatocytes were isolated according to established protocols [4546] and cultured in William's E medium with 5% BSA. AML and HEK293T cells were originally obtained from ATCC and cultured in Dulbecco's Modified Eagle Medium (DMEM) supplemented with 10% fetal bovine serum (FBS). SCAP$^{-/-}$ HEK293T cells were kindly provided by Dr. Peter Espenshade (Johns Hopkins University School of Medicine, Baltimore, MD, USA), and were cultured in the above-mentioned culture medium additionally supplemented with 5 μg/ml cholesterol, 1 mM sodium mevalonate, and 20 μM oleic acid as described previously [47]. All cells were incubated at 37°C in a humidified incubator containing 5% CO_2.

Gene expression and immunoblot analysis

For gene expression analysis, total RNA was isolated using TRIzol reagent (Invitrogen) and reverse transcribed using a homemade RT, as we previously described [48]. cDNA was quantified by real-time PCR using SYBR Green Master Mix (Diagenode) on BioRad Real-time PCR instrument. Gene expression levels were determined by using a standard curve. Each gene was normalized to the housekeeping gene 36B4, β-actin, or GAPDH. Total cellular protein was isolated from approximately 300mg of frozen liver tissue or cells of a 6-well plate using RIPA lysis buffer with protease inhibitor cocktail (Roche). Protein concentration was determined by BCA assay (Invitrogen), diluted in Nupage loading dye (Invitrogen), heated at 80 °C for 5 min, and run on 4–12% NuPAGE Bis-Tris Gel (Invitrogen) at 200V for 30min. Proteins were transferred to 0.22μM nitrocellulose membranes (Invitrogen) for 1 hr at 100V on ice and blocked with 5% milk in TBS-T to quench nonspecific protein binding. Samples were blotted with the indicated primary antibodies and detected using Alexa-488, Alexa-647, or IgG HRP-conjugated secondary antibodies.

Lipid quantification

For lipidomics analysis, 50–100 mg of frozen liver were homogenized in cold phosphate-buffered saline (PBS) using the Omni Bead Ruptor Elite with 2 mL homogenizer tube system (Omni, 19–628D) for 3 cycles of 10 s each at 5 m/s with a 10 s dwell time between cycles [49]. A total of 3–6 mg of homogenized material were applied to a modified Bligh and Dyer extraction. Prior to biphasic extraction, a 13 lipid class Lipidyzer Internal Standard Mix is added to each sample (AB Sciex, 5040156). Following two successive extractions, pooled organic layers are dried down in a Genevac EZ-2 Elite. Lipid samples are resuspended in 1:1 methanol/dichloromethane with 10 mM ammonium acetate and transferred to robovials (Thermo 10800107) for analysis. Samples were analyzed on the Sciex Lipidyzer Platform for targeted quantitative measurement of 1100 lipid species across 13 lipid sub-classes. Differential Mobility Device on Lipidyzer is tuned with SelexION tuning kit (Sciex 5040141). Instrument settings, tuning settings, and MRM list available upon request. Data analysis performed on Lipidyzer software. Quantitative values are normalized to milligrams of material used. For NAFLD model tissue lipids were measured by Folch extraction [46]. Tissue and serum triglycerides and cholesterol were quantified using commercially available enzymatic kits (Wako L-type TG M, Wako cholesterol E) according

to manufacturer's protocol. Oil Red O histochemistry staining were performed using frozen sections from mouse liver. Briefly, frozen sections were fixed in 10% neutral formalin for 10 min, followed by treatment in 60% isopropanol for 5 s and then staining in Oil Red O working solution (O-0625, Sigma Aldrich) for 15 min. This procedure was followed by washing with 60% isopropanol for 5 s and then water 1 min. Finally, sections were contained with Mayer's Hematoxylin for 3 min. Immunohistochemical staining of paraffin-embedded livers was performed by the UCLA Translational Pathology Core Laboratory (TPCL).

RNA-sequencing

Approximately 500μg of total RNA was isolated from frozen liver tissue of male and female mice fed chow, western, or high fat diet for 2 or 4 weeks (n=5 per group) using TRIzol reagent. mRNA was purified from each sample using Oligo(dT) Dynabeads (Invitrogen) and subjected to first strand cDNA synthesis and library prep using TruSeq stranded mRNA library prep kit (Illumina)and sequenced on an Illumina HiSeq 3000 with single-end 50-bp read length. Sequencing was performed by UCLA Technology Center for Genomics and Bioinformatics. The STAR ultrafast universal RNA-seq aligner v2.6d [50] was used to align the reads to a genome index that included both the genome sequence (GRCm38 mouse primary assembly) and the exon/intron structure of known mouse gene models (Gencode M18 genome annotation). Alignment files were used to generate strand-specific, gene-level count summaries with STAR's built-in gene counter. Independent filtering was applied as follows: genes with less than an average of 1 count per sample, count outliers or low mappability (<50bp) were filtered out for downstream analysis [51,52]. For the diet study, an additional in-house batch-correction step was implemented to correct for technical variability between libraries prepared at different times during the course of the project. Briefly, we employed one batch of samples comprising 5 independent replicates of the same condition to model and impute counts in other batches keeping the mean and dispersion distributions similar across batches. Expression estimates were computed in units of fragments per kilobase of mappable length and million counts (FPKMs). Count-based normalized and variance-stabilized data was used for all ordination, differential and clustering analyses, and all figures unless otherwise noted. Principal component analysis was performed with the function prcomp in R (https://www.R-project.org/) using standardize data as input. Samples hierarchical clustering was performed in Matlab (MATLAB, version release 2017a, The MathWorks, Inc, RRID:SCR_001622) using the pdist and seqlinkage functions. Differential expression analyses was performed with DESeq2 (Bioconductor, v3.7, RRID:SCR_015687)[52]. Several types of differential tests were performed. We used pair-wise contrasts for comparisons between levels of the same variable in a given group (e.g western diet vs. chow in males). In addition, count data were fitted to different types of multivariate models. For the diet dataset, we fitted the data to additive (~Sex+Diet) and interaction models (~Sex+Diet+Sex:Diet), and perform contrast tests with reduced models to evaluate the global effect of a variable or interaction between variables while controlling for baseline differences in the remaining variables. The same strategy was employed for the L-*Mettl14*KO dataset with Sex and *Mettl14* genotype as covariates. For each test, genes were classified as differential if adjusted p-value<0.01 (Wald test for pairwise contrasts, likelihood ratio test for multivariate models), with additional thresholds for size effect (log2 fold > 1) and baseline gene expression (FPKM>1). The pool of most variable genes in

each dataset, selected by PCA loadings or differential expression tests, was then subjected to model-based clustering using MBCluster.Seq[53] to classify them based on their overall abundance profile across samples. Functional enrichment for genes selected in the tests and clusters above was performed with Metascape [54]. All figures were generated in Matlab (MATLAB, version release 2017a, The MathWorks, Inc, RRID:SCR_001622).

m^{6}A-sequnecing

We followed the protocol previously outlined here [55] with minor modifications. Approximately 500μg of total RNA was extracted from frozen liver tissue (n=5 per group) using TRIzol reagent and purified using Oligo(dT) Dynabeads (Invitrogen). Because the large amount of input RNA required, we pooled approximately 1μg of purified mRNA was from each animal for each treatment group (n=5 per group). Approximately 5μg of pooled mRNA was then fragmented in fragmentation buffer (10mM Tris-HCl, pH=7.0, 10mM $ZnCl_2$) at 94°C for 2 min and 15 sec. 500ng mRNA (100ng per animal each group, pooled) was saved as input control for RNA-seq. 5μg of fragmented mRNA was incubated with 12μg of anti-m^{6}A antibody (Synaptic Systems) in 1X IP buffer (10mM Tris-HCl pH=7.4, 150mM NaCl, and 0.1% Igepal CA-630) for 2hr at 4°C on a rotating wheel. While fragmented mRNA was incubating, Protein A/G magnetic beads (Pierce) were washed twice and blocked by incubating in 1X IP buffer supplemented with 0.5mg/mL BSA for 2hr at 4°C on a rotating wheel. The m^{6}A-IP mixture was then added to the beads and incubated for an additional 2hr at 4°C on a rotating wheel. After 3 washes with IP buffer, bound mRNA was eluted by incubating with 100μL elution buffer (6.7mM N^6-Methyladenosine-5'-monophosphate salt in 1X IP buffer) for 1 hr at 4°C on a rotating wheel. Eluted mRNA fragments were collected, and the beads were incubated with an additional 100μL elution buffer for 1 hr at 4°C on a rotating wheel. The two 100μL eluates were combined and precipitated overnight at −20°C by adding one-tenth volume of 3M sodium acetate (pH=5.2) and 2.5 volumes of 100% ethanol. On average, 5μg of purified mRNA yielded tens of nanograms of immunoprecipitated mRNA fragments. Input and immunoprecipitated RNA fragments were subjected to first-strand cDNA synthesis and library prep using TruSeq stranded mRNA library prep kit (Illumina) and sequenced on an Illumina HiSeq 3000 with single-end 50-bp read length. Raw sequence files were aligned to the GRCm38 assembly of the mouse genome using the RNA-Seq pipeline above. Peak detection was performed using MACS2 (version 2.1.1) on uniquely aligned reads using default parameters except for the --nomodel flag (--extsize=200). Both enriched and depleted peaks (using the IP libraries as reference) were identified, pooled and consolidated into a single peak library. Both enriched and depleted peaks (using the IP libraries as reference) were identified using a q-value lower than 0.05, pooled and consolidated into a single peak library. Downstream peak normalization and analysis was performed on the merged set of significant m^{6}A peaks using variance stabilized data. Peak annotation was performed with PeakAnalyzer[56], and motif enrichment with the MEME suite[57]. Peak counts per sample were summarized with STAR's built-in gene counter by re-mapping the raw sequencing files to the peak database. Downstream differential peak analyses and normalization followed the same rules as for the RNA-Seq data.

m^{6}A-IP-qPCR

The relative abundance of select lipogenic mRNAs in m^{6}A antibody IP samples was assessed by RT-qPCR in mouse liver. Total RNA was isolated from frozen mouse liver using TRIzol (Invitrogen). After DNase treatment, RNA was fragmented in fragmentation buffer (50mM Tris-HCl, pH 8.0, 50mM $MgCl_2$) at 94 for 3 mins. A portion of fragmented RNA was saved as input control, and the remaining fragmented RNA (approximately 10μg of total RNA) was used to perform m^{6}A-IP-qPCR. m^{6}A-immunoprecipitation was performed as described in the m^{6}A-seq procedure. Approximately 300μg of total RNA was used to perform m^{6}A-IP-qPCR. A 300ng aliquot was saved and used as input control. The remaining RNA was used m^{6}A-immunoprecipitation as described in the m^{6}A-seq procedure. After overnight ethanol precipitation of immunoprecipitated RNAs, resulting pellets were suspended in 15μL RNase-free water and analyzed by qPCR. Abundance of lipogenic mRNAs in m^{6}A antibody samples was determined by normalizing to input control for each gene and expressed as the IP/input ratio or the % input.

mRNA half-life studies

Primary hepatocytes were treated with actinomycinD (5μg/mL, Sigma) for 0h, 2h and 4h before trypsinization and collection. Total RNA was isolated by TRIzol, reverse transcribed, and analyzed by qPCR. The degradation rate of RNA was estimated as previously described using Equation 1 and Equation 2 [13]:

$$\log_2(A_t/A_0) = -kt \quad \text{Equation 1:}$$

where t is transcription inhibition time (h), A_t and A_0 represent mRNA quantity at time t and time 0. Two k values were calculated: time 2h versus time 0h, and time 4h versus time 0h. The final lifetime was calculated by using the average of k_{2h} and k_{4h}:

$$t_{1/2} = 2\ln 2/(k_{2h} + k_{4h}) \quad \text{Equation 2:}$$

Polysome profiling

Total cellular protein was isolated from approximately 300mg of frozen liver tissue in 500μL of lysis buffer (10mM Tris, pH=7.4, 150mM KCl, 5mM $MgCl_2$, 100μg/mL CHX, 0.5% Triton-X-100, 1:100 protease inhibitor (Roche), 40U/mL SUPERasin). Extracts were left on ice for 15 min and then centrifuged at 15,000×g for 15 min at 4°C. Supernatant was collected (~0.5 ml) and a small aliquot (25μL) was used to measure absorbance at 260 nm. Lysis buffer was used to equalize samples by A_{260} units. Each lysate was then split by ratio of 1:4 (Portion I/Portion II). 1 mL Trizol was added to Portion I and RNA was isolated to serve as input RNA. A 10/50% w/v sucrose gradient was prepared in lysis buffer without Triton-X. Portion II (~375μL) was then layered onto the top of the sucrose gradient by dispensing slowly down the side of tube, making sure not to disturb gradient. Gradients were then centrifuged at 4 °C for 4 h at 27,500 r.p.m. (Beckman, rotor SW28). Aliquots of 250μL were then collected starting from the top of gradient and absorbance measured at 260nm on a nanospectrometer. Aliquots were then categorized into 3 main sub-types using the curve generated in the previous step (non-ribosome portion, 40S-80S, and polysome). Each aliquot

was then combined with an equal volume of TRIzol to purify RNA and used for qPCR analysis. Abundance of lipogenic mRNAs in each fraction was determined by normalizing to input control value for each gene. We also performed the analysis by normalizing to housekeeper within the same fraction which did not alter the results.

Mitochondrial isolation and bioenergetics

Briefly, liver was minced, washed with PBS, and homogenized with glass Dounce homogenizer. Mitochondria were isolated by dual centrifugation (800 g and 8000 g) and respiration was obtained with a Seahorse bioanalyzer XF24 (Agilent) [58]. Fatty acid oxidation was measured in presence of 60 μM palmitoyl-carnitine, 250 μM malate and 4 μM FCCP.

ATAC-seq

ATAC-seq was optimized in liver after several modifications from original Buenstero et al. protocol [49]. A total of 100 mg of frozen liver were grinded to fine powder using cellcrusher and 1 mL of ice cold nuclei isolation buffer was added (20 mM Tris-HCl, 50 mM EDTA, 5 mM spermidine, 0.15 mM spermine, 0.1% mercaptoethanol, 40% glycerol, pH 7.5, mM EGTA, and 60 mM KCl). After 5 min of cooling on ice, cell suspension was filtered through Miracloth (Calbiochem) followed by centrifugation at 1100 × *g* for 10 min at 4 °C. Pellet was resuspended with 50 μL RSB buffer (10 mM Tris-HCl, 10 mM NaCl, 3 mM MgCl2, and pH 7.4) followed by centrifugation at 500 × *g* for 5 min at 4 °C and resuspension in PBS. A total of 75,000 nuclei pellet were used for transposase reaction. The rest of the protocol followed that described by Buenstero [49]. ATAC-Seq libraries were prepared using the Nextera Tn5 Transposase and DNA library preparation kit (Illumina) as described [49]. Libraries were single-end sequenced (50 bp) on an Illumina HiSeq 2000. Reads were mapped to the mouse genome (NCBI37/mm9) using Bowtie2 and were removed from the subsequent analysis if they were duplicated, mapped to mitochondrial genome, or aligned to unmapped contiguous sequences. Peak calling was performed using MACS2. The reads were converted to reads per thousand base pairs peak per million mapped reads (RPKM) by dividing by the total number of reads per sample. The average RPKM from four replicates was used to quantify the accessibility across all called peaks.

Single-molecule RNA FISH with fluorescent immunostaining:

Sequential RNA FISH with fluorescent immunostaining was performed in AML cells transiently transfected with scrambled shRNAs or shRNAs targeting Mettl14 [59]. After 48 hours, the cells were washed once in PBS and then fixed in 37% formaldehyde in PBST (PBS with 0.05% Tween-20) at room temperature for 15 min. The fixing solution was removed, and cold methanol was added to each chamber and incubated for 10 min at room temperature. Cells were rinsed once in PBS and incubated with blocking solution for 1 h at room temperature under rotation. After 1 h, the blocking solution was replaced with primary antibody (Mouse anti-DCP1a; WH0055802M6; Sigma; 1:300) and incubated for 1 h at room temperature (or overnight at 4 °C). After being washed 4 times with PBST (500 μl, 5–10 min for each wash), secondary antibody (Alexa 488 conjugate, 1:300 dilution in PBST) was added to the mixture and incubated at room temperature for 1 h. After washing 4 times with PBST (500 μl, 5–10 min for each wash), Stellaris FISH probe with Cal-Fluor610 were added

and incubated 4hr at 37 °C in the dark. After washing 4 times with PBST (500 μl, 5–10 min for each wash), anti-fade reagent (ProLong Diamond Antifade mountant with DAPI, Invitrogen) was added to mount the slides. The images were captured by a Zeiss LSM880 Confocal microscope with Airyscan and analyzed by ImageJ. Complete set of probes used provided in supplemental Table 3.

Targeted m^{6}A-modification of cellular mRNAs

TRM editor plasmid encoding nuclease-dead Cas13b and truncated Mettl3 fused to a nuclear localization sequence (pCMV-dCas13-M3nls) and gRNA expression plasmid (pU6-PspCas13b-gRNA) were obtained from Addgene (155366 and 155368; respectively). gRNAs targeting specific m^{6}A sites identified from m6A-seq on SCD1 mRNA as well as a nontargeting control gRNA were manufactured by IDT and gibson-cloned (NEB) into the gRNA expression plasmid. Targeted m^{6}A-modification of cellular mRNAs with TRM editors was then performed as previously described [26]. AML cells were plated on 6-well plates (for RNA) or 10-cm dishes (for protein and at approximately 80% confluency were transfected using Fugene HD (Promega) with 2.3μg of TRM editor plasmid and 1.1μg of gRNA expression plasmid (for 6-well) or 13.3μg of TRM editor plasmid and 5.7μg of gRNA expression plasmid (for 10-cm). At 48 hours post-transfection, protein and total RNA were harvested as described in the gene expression and immunoblot analysis section. The relative abundance of m^{6}A at different sites on *Scd1* mRNA in cells transfected with gRNAs targeting these sites or nontargeting control gRNAs was assessed by m^{6}A-IP-qPCR. To account for variability in RNA amounts, m^{6}A abundance at each site on *Scd1* was normalized to input or a nontargeted region on the TRM-edited transcript.

Statistical analysis

A non-paired Student’s t-test was used to determine statistical significance, defined at $P < 0.05$. For multiple group experiments analysis of variance was used followed by multiple group analysis. Unless otherwise noted, error bars represent standard error of mean. Most experiments were independently performed at least twice. Sample size is based on statistical analysis of variance and prior experience with similar in vivo studies.

Extended Data

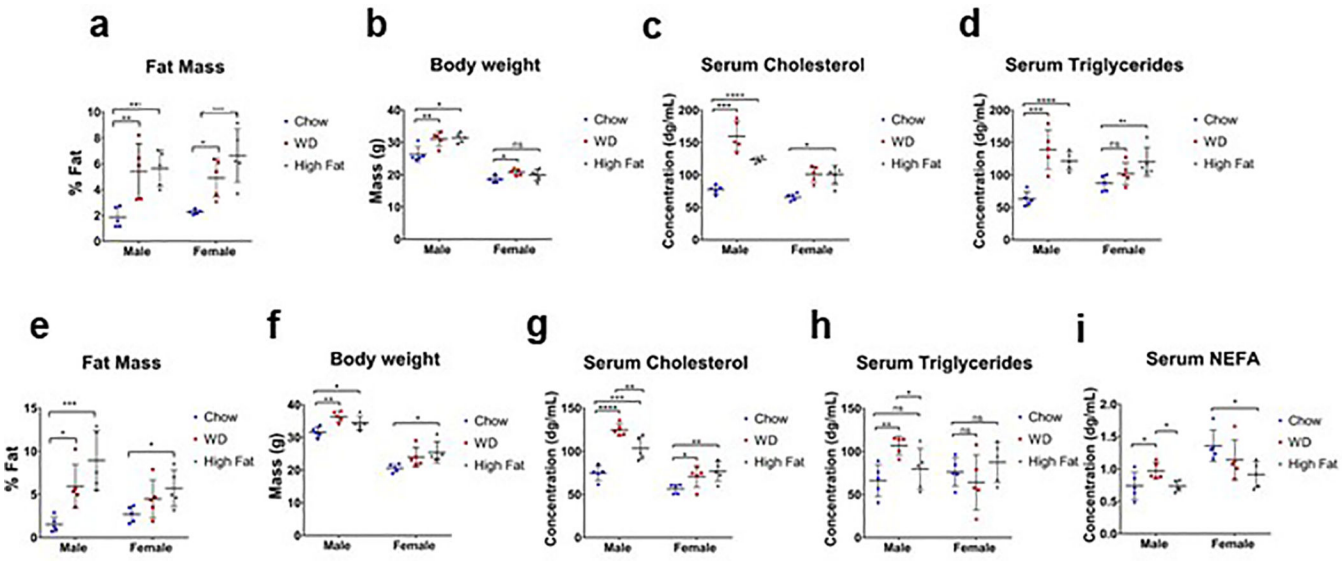

Extended Data Fig. 1. Effect of sex and diet composition on lipid metabolism.

a, Fat mass measured by MRI for male and female mice in 2week cohort *(n*=5 per group). **b,** Body weight of male and female mice in 2-week cohort *(n*=5 per group). **c,** Quantification of serum cholesterol levels of male and female mice in 2-week cohort *(n*=5 per group). **d,** Quantification of total serum triglycerides of male and female mice in 2-week cohort *(n*=5 per group). **e,** Fat mass measured by MRI for male and female mice in 4-week cohort *(n*=5 per group). **f,** Body weight of male and female mice in 4-week cohort *(n*=5 per group). **g,** Quantification of serum cholesterol levels of male and female mice in 4-week cohort *(n*=5 per group). **h,** Quantification of total serum triglycerides of male and female mice in 4-week cohort (*n*=5 per group). **i,** Quantification of total serum NEFA from male and female mice in 4-week cohort (*n*=5 per group). Mice were fed indicated diet for 4 weeks and fasted for 4-hrs. prior to sacrifice. Values are mean ± s.e.m. of 5 independent biological replicates (**a-i**). *P* values were calculated using one-way analysis of variance (ANOVA) with multi-group comparison (Fisher's) in **a-i**. **P<0.05;* ** *P<0.01;* *** *P<0.001;* **** *P<0.0001.* The precise *n, P* values, and details of the statistical testing are provided in the source data file.

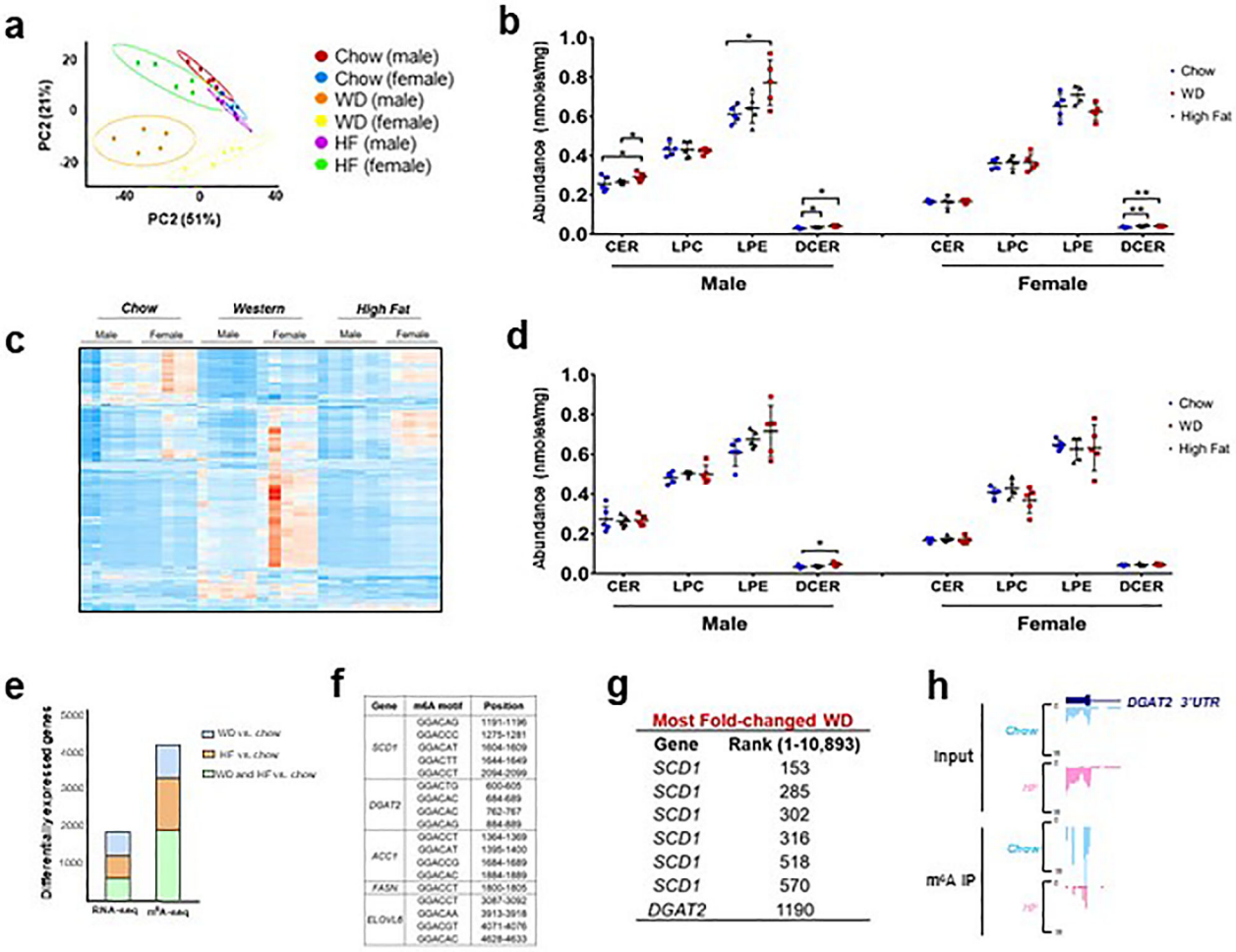

Extended Data Fig. 2. Lipogenic genes are highly enriched for m^{6}A under chow diet.

a, Lipidomics PCA plot for 4-week cohort (*n*=5 per group). **b,** Quantification of major lipid species identified in lipidomics analysis of male and female mouse liver for 2-week cohort (*n*=5 per group). **c,** Lipidomics heatmap for 4-week cohort (*n*=5 per group). **d,** Quantification of major lipid species identified in lipidomics analysis of mouse liver for 4-week cohort (*n*=5 per group). **e,** Comparison of number of differentially expressed genes (>2fold) in WD or HF versus chow-fed male livers determined by RNA-seq and m^{6}A-seq. **f,** Nucleotide sequences containing the m^{6}A motifs on lipogenic transcripts and relative position of each motif on full-length mRNA. **g,** Rank order table of genes with greatest fold-change in m^{6}A in male livers (Chow vs. Western diet). **h,** UCSC browser screenshot showing changes in m^{6}A enrichment for *DGAT2* in chow and HF diet-fed male livers. Mice were fed indicated diet for 4 weeks and fasted for 4-hrs. prior to sacrifice. Values are mean ± s.e.m. of 5 independent biological replicates (**b,d**). *P* values were calculated using one-way analysis of variance (ANOVA) with multi-group comparison (Fisher's) in **b** and **d**. **P<0.05;* ** *P<0.01;* *** *P<0.001;* **** *P<0.0001.* The precise *n, P* values, and details of the statistical testing are provided in the source data file.

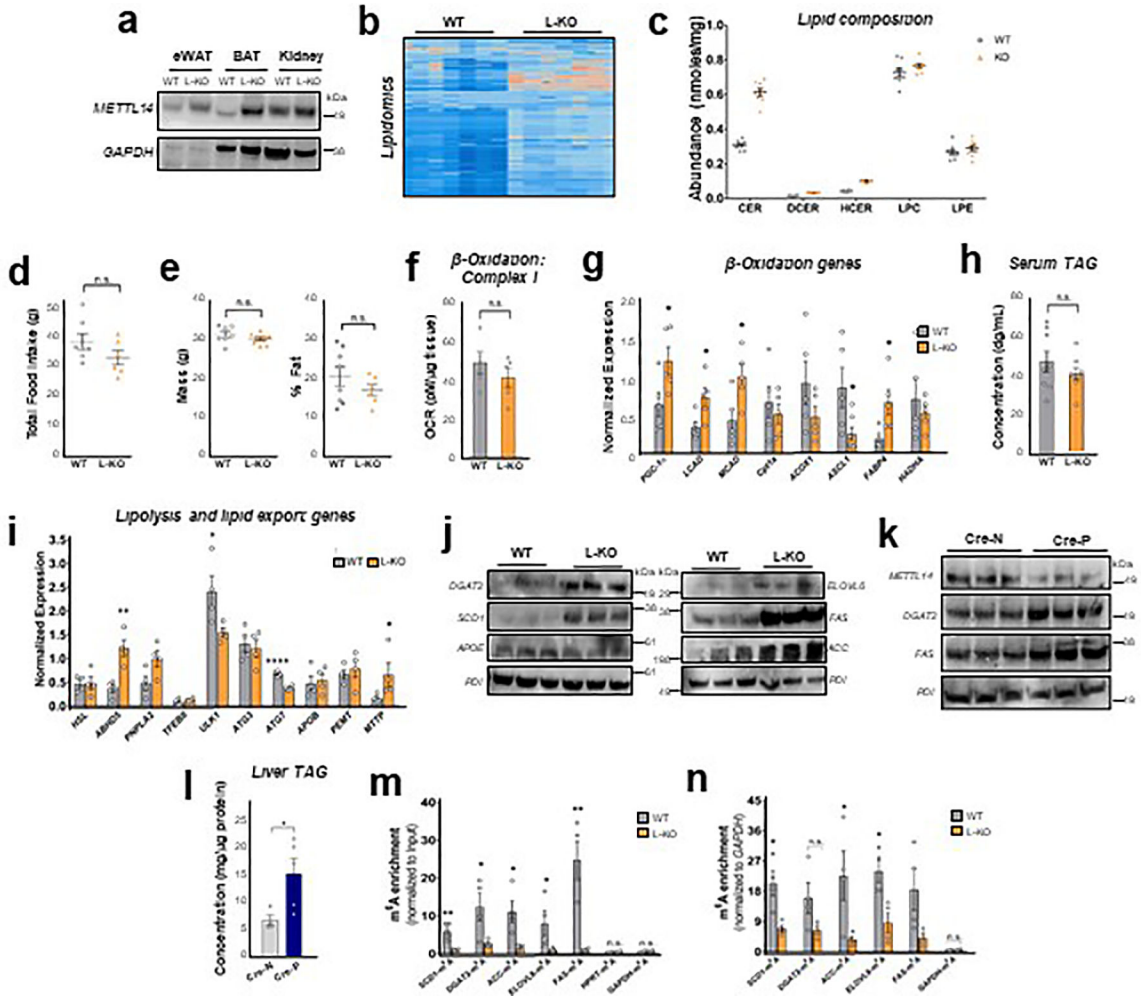

Extended Data Fig. 3. Loss of the m^{6}A methylase METTL14 increases lipogenesis and hepatic triglyceride accumulation.

a, Western blot of *Mettl14* in other tissues from WT and *Mettl14* L-KO chow-fed males. Equal amounts of protein were pooled from four animals per group and run in triplicate. **b,** Lipidomics heatmap comparing hepatic lipidome of WT versus *Mettl14* L-KO chow-fed males. (*n*=8 per group). **c,** Quantification of various lipid species from lipidomics analysis of chow-fed male livers (*n* = 8). Statistical analysis was performed using unpaired two-tailed *t*-test. Values are mean ± SEM. **d,** Quantification of total food intake for chow-fed male WT and *Mettl14* L-KO mice (*n*=8 per group). **e,** Body weight and percent fat measured by MRI for chow-fed male WT and *Mettl14* L-KO mice (*n* = 8 WT mice, *n* = 7 L-KO mice). **f,** Quantification of cellular respiratory rate in livers of chow-fed WT and *Mettl14* L-KO mice using NADH as the acceptor (*n*=5 per group). **g,** qPCR analysis of fatty acid oxidation gene expression from chow-fed WT and *Mettl14* L-KO livers (*n*=5). The experiment was repeated two times with similar results. **h,** Quantification of serum triglyceride levels from chow-fed male WT and *Mettl14* L-KO mice (*n*=8 per group). **i,** qPCR analysis of gene expression from liver of WT and *Mettl14* L-KO mice (*n*=4 per group). The experiment was repeated two times with similar results. **j,** Western blot of lipogenic protein levels in a second independent cohort of chow-fed male mice. Equal amounts of protein were pooled

from eight animals per group and run in triplicate. The experiment was repeated three times with similar results. **k,** Western blot comparing levels of lipogenic proteins in the setting of chronic *Mettl14* deficiency (albumin-cre transgenics or control). Equal amounts of protein were pooled from five animals per group and run in triplicate. The experiment was repeated two times with similar results. **l,** Quantification of hepatic triglyceride concentrations from livers of albumin-cre transgenic or control mice (n = 4 Cre-N mice, n = 5 Cre-P mice). **m,** Quantification of lipogenic transcript m^{6}A abundance in WT and *Mettl14* L-KO chow-fed livers measured by m^{6}A-IP-qPCR analysis (n = 4). The relative enrichment of m^{6}A in each sample was determined by normalizing to ten-fold input. The experiment was repeated two times with similar results. **n,** Quantification of lipogenic transcript m^{6}A abundance in WT and *Mettl14* L-KO chow-fed livers measured by m^{6}A-IP-qPCR analysis (n=4). The relative enrichment of m^{6}A in each sample was determined by normalizing to *GAPDH.* The experiment was repeated two times with similar results. Mice were fed chow diet for 4 weeks and fasted for 4-hrs. prior to sacrifice. Values are mean ± s.e.m. of 4 (**I,l-n**), 5 (**f,g**), 6 (**d**), or 8 (**c,e,h**) independent biological replicates. P values were calculated using unpaired two-tailed t-test. (**c-i,l-n**). *$P<0.05$; ** $P<0.01$; *** $P<0.001$; **** $P<0.0001$. The precise n, P values, and details of the statistical testing are provided in the source data file.

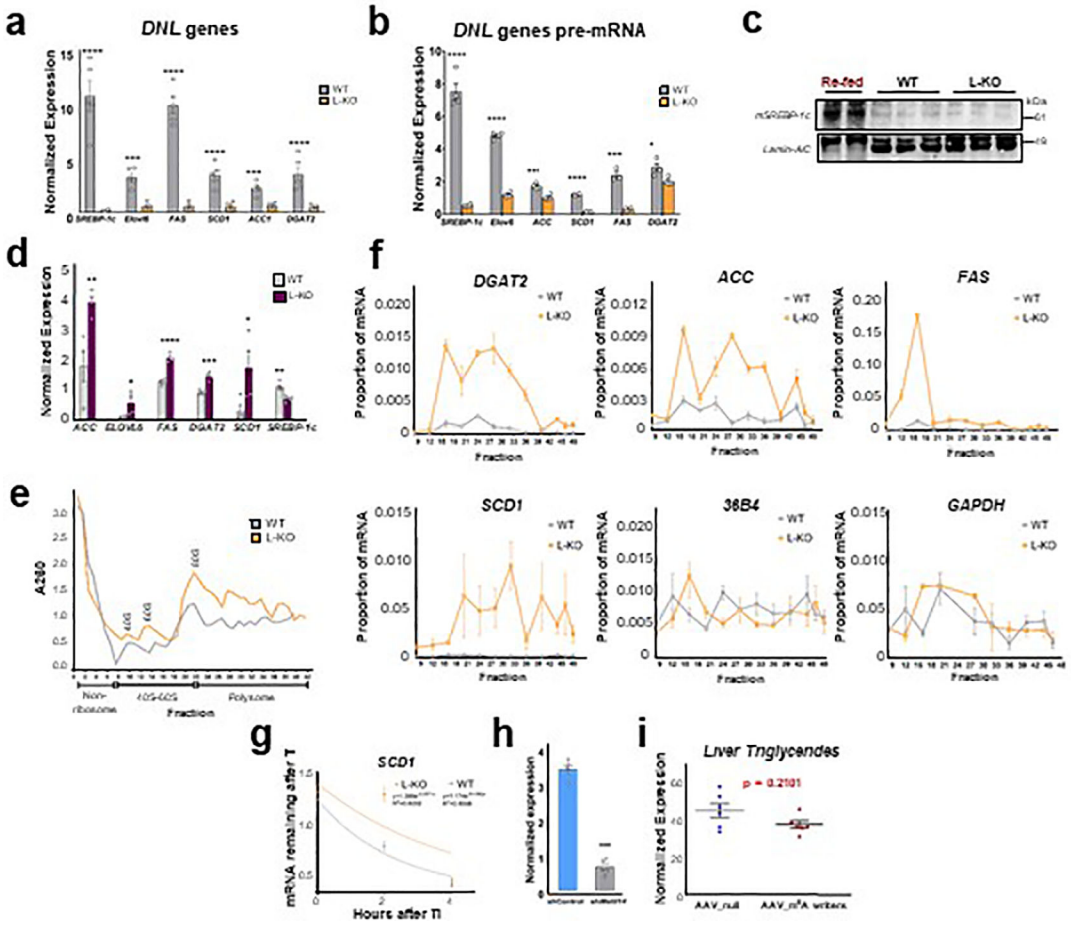

Extended Data Fig. 4. m^{6}A regulates the stability and cytoplasmic distribution of lipogenic transcripts.

a, qPCR analysis of lipogenic gene expression in livers of WT and *Mettl14* L-KO chow-fed male mice *(n*=6 per group). The experiment was repeated three times with similar results. **b,** qPCR analysis of lipogenic pre-mRNA expression using primers that amplify intronic regions from livers of WT and *Mettl14* LKO chow-fed male mice *(n*=4 per group). The experiment was repeated three times with similar results. **c,** Western blot of SREBP-1c from nuclear fraction (mature SREBP-1 [mSREBP1c]). mSREBP-1c levels in livers of re-fed (4 hr.) mice are shown as reference. Equal amounts of protein were pooled from five animals per group and run in triplicate. The experiment was repeated two times with similar results **d,** qPCR analysis of lipogenic transcript levels in WT or *Mettl14* LKO livers at 72 hrs. after *Mettl14* deletion *(n*=4). **e,** Polysome profiling curve depicting three major cytoplasmic mRNA pools. **f,** qPCR analysis quantifying amount of lipogenic mRNAs in ribosome-bound fractions in livers of *Mettl14* L-KO chow-fed males compared to WT *(n*=3 per group). **g,** mRNA stability assay for *SCD1* mRNA in primary hepatocytes harvested from WT and *Mettl14* L-KO chow-fed male mice *(n* = 3 per group). **h,** qPCR analysis of *Mettl14* expression in AML cells used for single-molecule RNA FISH. *(n* = 5 per group). **i,** Quantification of hepatic triglyceride content in WD-fed male mice injected with AAV_m^{6}A writers (*Mettl14*+*Mettl3*+*WTAP*) or AAV_null (normalized to liver weight) *(n*=6 per group). Mice were fed indicated diet for 4 weeks and fasted for 4-hrs. prior to sacrifice except for mice in (**i**). Mice in (**i**) were fed NASH diet for 8-weeks and fasted 4-hrs. prior to sacrifice. Values are mean ± s.e.m. of 3 (**f,g**), 4 (**b,d**), 5 (**h**), or 6 (**a,i**) independent biological replicates. *P* values were calculated using unpaired two-tailed *t*-test. (**a,b,d,h,i**). **P<0.05; ** P<0.01; *** P<0.001; **** P<0.0001.* The precise *n, P* values, and details of the statistical testing are provided in the source data file.

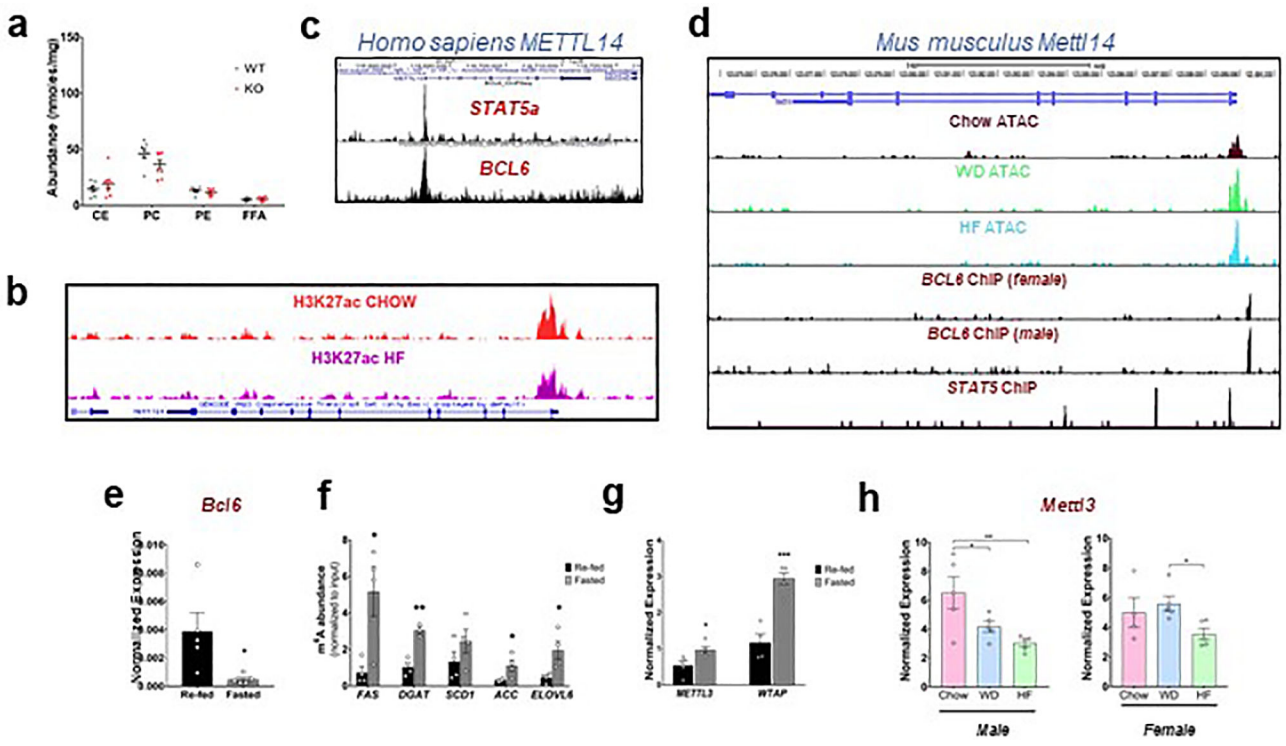

Extended Data Fig. 5. Regulation of *Mettl14* in response to dietary conditions

a, Quantification of major lipid species identified in lipidomics analysis of male WD-fed WT and *Mettl14* L-KO livers (*n* = 7 WT mice, *n* = 8 KO mice). **b,** UCSC browser screenshots showing decreased H3K27ac at *Mettl14* promoter under HF diet feeding compared to chow. Mice were fed either standard chow diet (Prolab Isopro RMH 3000, Purina) for 24 weeks or 8 weeks of standard chow diet followed by 16 weeks of HFD (Soltis *et al.* 2017. *Cell Reports*). **c,** UCSC browser screenshots showing regulation of *METTL14* promoter by *BCL6* and *STAT5a in human (*Steube *et. al* 2017. *Nat Comm;* Gertz *et. al* 2013. *Mol. Cell; respectively*). **d,** UCSC browser screenshots showing ATAC-seq data for *Mettl14* promoter region from male mouse liver under different diets and regulation of *Mettl14* promoter by *BCL6 and STAT5a* in male and female mice fed WD (Zhang *et. al* 2011. *Mol Cel Biol*). **e,** qPCR analysis showing fast/refeed regulation of *Bcl6* expression in livers of chow-fed males (*n*=5 per group). The experiment was repeated twice with similar results. **f,** Quantification of m^6A abundance on lipogenic transcripts in fasted (4 hr) or re-fed (fasted overnight and then re-fed 4 hr) male livers as measured by m^6A-IP-qPCR (*n*=4). The experiment was repeated twice with similar results. **g,** Expression of *Mettl3, WTAP* in re-fed mice (fasted overnight and then re-fed 4 hr) compared to fasted (4 hr) mice as measured by qPCR analysis (*n*=5). **h,** qPCR analysis of *Mettl3* expression in male and female liver under various diets (*n* = 4 chow-fed females, *n* = 5 all other groups). Mice were fed the indicated diet for 4 weeks and fasted (4 hr) or re-fed (fasted overnight and then refed for 4-hrs. prior to sacrifice). Values are mean ± s.e.m. of 4 (**f**), 5 (**e,g,h**) or 7 (**a**) indpendent biological replicates. *P* values were calculated using unpaired two-tailed *t*-test (**a,e-g**) or one-way analysis of variance (ANOVA) followed by multi-group comparison (Fisher's) in **h**. **P<0.05;* ** *P<0.01;* *** *P<0.001;* **** *P<0.0001*. The precise *n, P* values, and details of the statistical testing are provided in the source data file.

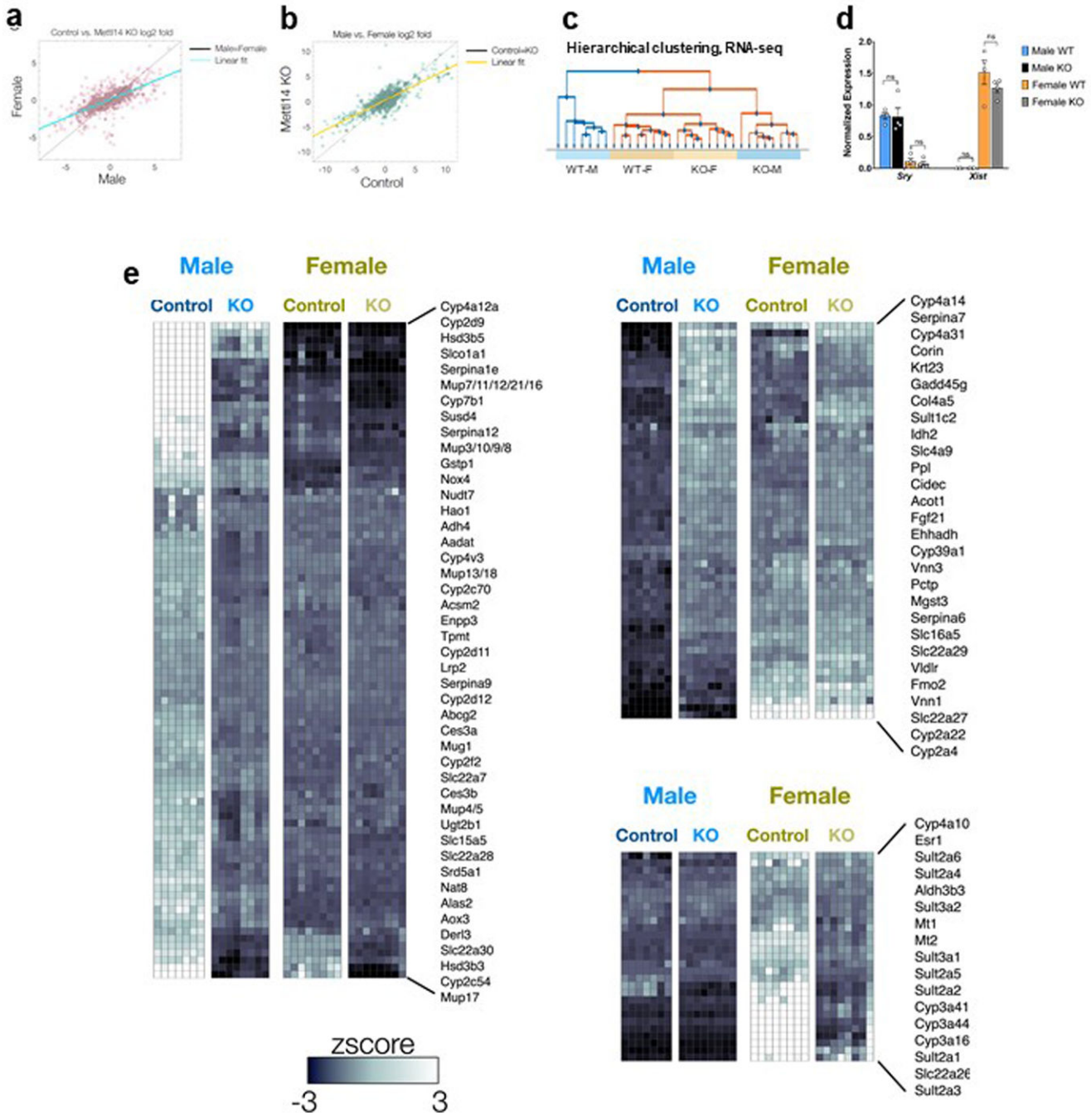

Extended Data Fig. 6. Loss of *Mettl14* is associated with sexbiased gene expression.

a, Comparison of gene expression fold changes between control and *Mettl14* L-KO mice obtained from male (x axis) or female (y axis) samples. **b,** Comparison of gene expression fold changes between male and female mice obtained from control (x axis) or *Mettl14* L-KO (y axis) samples. The linear fit of all fold changes (yellow) has a smaller slope than the Control=KO line (black), highlighting that male/female differences are higher in controls for most genes. **c,** Hierarchical clustering of samples harvested from liver based on pair-wise distances. Shown is the tree based on the Euclidean distance between all samples ($n = 7$

WT male mice, $n = 8$ mice all other groups) based on genome-wide mRNA abundance distributions**. d,** Expression of *XIST* and *SRY* in livers of WT and *Mettl14* L-KO mice as measured by qPCR ($n = 4$)**. e,** Heatmaps of selected differential genes with distinct responses to *Mettl14* L-KO. Three specific clusters of genes with sex-specific response to *Mettl14* are shown. Highlighted are the name of genes known to be involved in metabolic pathways. Gene names are ordered as in the heatmap. All mice were fed WD for 4 weeks and fasted for 4 hrs. prior to sacrifice. *P* values were calculated using unpaired two-tailed *t*test (**d**). The precise *n, P* values, and details of the statistical testing are provided in the source data file.

Supplementary Material

Refer to Web version on PubMed Central for supplementary material.

Acknowledgements:

This work was supported by NIH grants DK118086 (T.S.), HL139549(T.S.), HL149766(T.S.), NS111631 (S.J), CA186702 (S.J), CA236399 (J.C), CA214965 (J.C.), and CA243386 (J.C.), American Heart Association Transformational Project grant (T.S.) and Burroughs Wellcome Fund Career Award for Medical Scientists (T.S). J.C. J.C. is a Leukemia &Lymphoma Society (LLS) Scholar. Schematic for figures created with BioRender.com

References

1. Horton JD, Goldstein JL & Brown MS SREBPs: activators of the complete program of cholesterol and fatty acid synthesis in the liver. The Journal of clinical investigation 109, 1125–1131, doi:10.1172/JCI15593 (2002). [PubMed: 11994399]
2. Shimomura Iet al.Insulin selectively increases SREBP-1c mRNA in the livers of rats with streptozotocin-induced diabetes. Proc Natl Acad Sci U S A96, 13656–13661, doi:10.1073/pnas.96.24.13656 (1999). [PubMed: 10570128]
3. Shimano Het al.Isoform 1c of sterol regulatory element binding protein is less active than isoform 1a in livers of transgenic mice and in cultured cells. J Clin Invest99, 846–854, doi:10.1172/JCI119248 (1997). [PubMed: 9062341]
4. Lee KN, Pariza MW & Ntambi JM Differential expression of hepatic stearoyl-CoA desaturase gene 1 in male and female mice. Biochim Biophys Acta 1304, 85–88, doi:10.1016/s0005-2760(96)00145-2 (1996). [PubMed: 8954132]
5. Horton JD, Shimano H, Hamilton RL, Brown MS & Goldstein JL Disruption of LDL receptor gene in transgenic SREBP-1a mice unmasks hyperlipidemia resulting from production of lipid-rich VLDL. J Clin Invest 103, 1067–1076, doi:10.1172/JCI6246 (1999). [PubMed: 10194480]
6. Roundtree IA, Evans ME, Pan T & He C Dynamic RNA Modifications in Gene Expression Regulation. Cell 169, 1187–1200, doi:10.1016/j.cell.2017.05.045 (2017). [PubMed: 28622506]
7. Frye M, Harada BT, Behm M & He C RNA modifications modulate gene expression during development. Science 361, 1346–1349, doi:10.1126/science.aau1646 (2018). [PubMed: 30262497]
8. Meyer KD & Jaffrey SR The dynamic epitranscriptome: N6-methyladenosine and gene expression control. Nat Rev Mol Cell Biol 15, 313–326, doi:10.1038/nrm3785 (2014). [PubMed: 24713629]
9. Zaccara S, Ries RJ & Jaffrey SR Reading, writing and erasing mRNA methylation. Nat Rev Mol Cell Biol 20, 608–624, doi:10.1038/s41580-019-0168-5 (2019). [PubMed: 31520073]
10. Wang Xet al.N6-methyladenosine-dependent regulation of messenger RNA stability. Nature505, 117–120, doi:10.1038/nature12730 (2014). [PubMed: 24284625]
11. Engel Met al.The Role of m(6)A/m-RNA Methylation in Stress Response Regulation. Neuron99, 389–403 e389, doi:10.1016/j.neuron.2018.07.009 (2018). [PubMed: 30048615]
12. Linder Bet al.Single-nucleotide-resolution mapping of m6A and m6Am throughout the transcriptome. Nat Methods12, 767–772, doi:10.1038/nmeth.3453 (2015). [PubMed: 26121403]

13. Weng Het al.METTL14 Inhibits Hematopoietic Stem/Progenitor Differentiation and Promotes Leukemogenesis via mRNA m(6)A Modification. Cell Stem Cell22, 191–205 e199, doi:10.1016/j.stem.2017.11.016 (2018). [PubMed: 29290617]
14. Liu Jet al.N (6)-methyladenosine of chromosome-associated regulatory RNA regulates chromatin state and transcription. Science367, 580–586, doi:10.1126/science.aay6018 (2020). [PubMed: 31949099]
15. Sun Zet al.Hepatic Hdac3 promotes gluconeogenesis by repressing lipid synthesis and sequestration. Nat Med18, 934–942, doi:10.1038/nm.2744 (2012). [PubMed: 22561686]
16. Lu Met al.Insulin regulates liver metabolism in vivo in the absence of hepatic Akt and Foxo1. Nat Med18, 388–395, doi:10.1038/nm.2686 (2012). [PubMed: 22344295]
17. Ries RJet al.m(6)A enhances the phase separation potential of mRNA. Nature571, 424–428, doi:10.1038/s41586-019-1374-1 (2019). [PubMed: 31292544]
18. Zaccara S & Jaffrey SR A Unified Model for the Function of YTHDF Proteins in Regulating m(6)A-Modified mRNA. Cell 181, 1582–1595 e1518, doi:10.1016/j.cell.2020.05.012 (2020). [PubMed: 32492408]
19. Attie ADet al.Relationship between stearoyl-CoA desaturase activity and plasma triglycerides in human and mouse hypertriglyceridemia. J Lipid Res43, 1899–1907, doi:10.1194/jlr.m200189-jlr200 (2002). [PubMed: 12401889]
20. Ou Jet al.Unsaturated fatty acids inhibit transcription of the sterol regulatory element-binding protein-1c (SREBP-1c) gene by antagonizing ligand-dependent activation of the LXR. Proc Natl Acad Sci U S A98, 6027–6032, doi:10.1073/pnas.111138698 (2001). [PubMed: 11371634]
21. Dentin Ret al.Polyunsaturated fatty acids suppress glycolytic and lipogenic genes through the inhibition of ChREBP nuclear protein translocation. J Clin Invest115, 2843–2854, doi:10.1172/JCI25256 (2005). [PubMed: 16184193]
22. Matsuda Met al.SREBP cleavage-activating protein (SCAP) is required for increased lipid synthesis in liver induced by cholesterol deprivation and insulin elevation. Genes Dev15, 1206–1216, doi:10.1101/gad.891301 (2001). [PubMed: 11358865]
23. Shao W, Machamer CE & Espenshade PJ Fatostatin blocks ER exit of SCAP but inhibits cell growth in a SCAP-independent manner. J Lipid Res 57, 1564–1573, doi:10.1194/jlr.M069583 (2016). [PubMed: 27324795]
24. Xiong Xet al.Landscape of Intercellular Crosstalk in Healthy and NASH Liver Revealed by Single-Cell Secretome Gene Analysis. Mol Cell75, 644–660 e645, doi:10.1016/j.molcel.2019.07.028 (2019). [PubMed: 31398325]
25. Kleiner DEet al.Design and validation of a histological scoring system for nonalcoholic fatty liver disease. Hepatology41, 1313–1321, doi:10.1002/hep.20701 (2005). [PubMed: 15915461]
26. Wilson C, Chen PJ, Miao Z & Liu DR Programmable m(6)A modification of cellular RNAs with a Cas13-directed methyltransferase. Nat Biotechnol, doi:10.1038/s41587-020-0572-6 (2020).
27. Liu XM, Zhou J, Mao Y, Ji Q & Qian SB Programmable RNA N(6)-methyladenosine editing by CRISPR-Cas9 conjugates. Nat Chem Biol 15, 865–871, doi:10.1038/s41589-019-0327-1 (2019). [PubMed: 31383972]
28. Link JCet al.X chromosome dosage of histone demethylase KDM5C determines sex differences in adiposity. J Clin Invest, doi:10.1172/JCI140223 (2020).
29. Buenrostro JD, Giresi PG, Zaba LC, Chang HY & Greenleaf WJ Transposition of native chromatin for fast and sensitive epigenomic profiling of open chromatin, DNA-binding proteins and nucleosome position. Nature methods 10, 1213–1218, doi:10.1038/nmeth.2688 (2013). [PubMed: 24097267]
30. Sommars MAet al.Dynamic repression by BCL6 controls the genome-wide liver response to fasting and steatosis. Elife8, doi:10.7554/eLife.43922 (2019).
31. Senagolage MDet al.Loss of Transcriptional Repression by BCL6 Confers Insulin Sensitivity in the Setting of Obesity. Cell Rep25, 3283–3298 e3286, doi:10.1016/j.celrep.2018.11.074 (2018). [PubMed: 30566857]
32. Kutyavin VI & Chawla A BCL6 regulates brown adipocyte dormancy to maintain thermogenic reserve and fitness. Proc Natl Acad Sci U S A 116, 17071–17080, doi:10.1073/pnas.1907308116 (2019). [PubMed: 31375635]

33. Zhang Y, Laz EV & Waxman DJ Dynamic, sex-differential STAT5 and BCL6 binding to sex-biased, growth hormone-regulated genes in adult mouse liver. Mol Cell Biol 32, 880–896, doi:10.1128/MCB.06312-11 (2012). [PubMed: 22158971]
34. Connerney J, Lau-Corona D, Rampersaud A & Waxman DJ Activation of Male Liver Chromatin Accessibility and STAT5-Dependent Gene Transcription by Plasma Growth Hormone Pulses. Endocrinology 158, 1386–1405, doi:10.1210/en.2017-00060 (2017). [PubMed: 28323953]
35. Qasem RJet al.Decreased liver triglyceride content in adult rats exposed to protein restriction during gestation and lactation: role of hepatic triglyceride utilization. Clin Exp Pharmacol Physiol42, 380–388, doi:10.1111/1440-1681.12359 (2015). [PubMed: 25641378]
36. Zhang Wet al.FoxO1 regulates multiple metabolic pathways in the liver: effects on gluconeogenic, glycolytic, and lipogenic gene expression. J Biol Chem281, 10105–10117, doi:10.1074/jbc.M600272200 (2006). [PubMed: 16492665]
37. Link JC & Reue K Genetic Basis for Sex Differences in Obesity and Lipid Metabolism. Annu Rev Nutr 37, 225–245, doi:10.1146/annurev-nutr-071816-064827 (2017). [PubMed: 28628359]
38. Rinn JL & Snyder M Sexual dimorphism in mammalian gene expression. Trends Genet 21, 298–305, doi:10.1016/j.tig.2005.03.005 (2005). [PubMed: 15851067]
39. Wang B & Tontonoz P Liver X receptors in lipid signalling and membrane homeostasis. Nat Rev Endocrinol 14, 452–463, doi:10.1038/s41574-018-0037-x (2018). [PubMed: 29904174]
40. Lonardo Aet al.Sex Differences in Nonalcoholic Fatty Liver Disease: State of the Art and Identification of Research Gaps. Hepatology70, 1457–1469, doi:10.1002/hep.30626 (2019). [PubMed: 30924946]
41. McIntyre ABRet al.Limits in the detection of m(6)A changes using MeRIP/m(6)A-seq. Sci Rep10, 6590, doi:10.1038/s41598-020-63355-3 (2020). [PubMed: 32313079]
42. Xu J, Teran-Garcia M, Park JH, Nakamura MT & Clarke SD Polyunsaturated fatty acids suppress hepatic sterol regulatory element-binding protein-1 expression by accelerating transcript decay. J Biol Chem 276, 9800–9807, doi:10.1074/jbc.M008973200 (2001). [PubMed: 11124951]
43. Sessler AM, Kaur N, Palta JP & Ntambi JM Regulation of stearoyl-CoA desaturase 1 mRNA stability by polyunsaturated fatty acids in 3T3-L1 adipocytes. J Biol Chem 271, 29854–29858, doi:10.1074/jbc.271.47.29854 (1996). [PubMed: 8939925]
44. Wang Xet al.Hepatocyte TAZ/WWTR1 Promotes Inflammation and Fibrosis in Nonalcoholic Steatohepatitis. Cell Metab24, 848–862, doi:10.1016/j.cmet.2016.09.016 (2016). [PubMed: 28068223]
45. Rong Xet al.LXRs regulate ER stress and inflammation through dynamic modulation of membrane phospholipid composition. Cell Metab18, 685–697, doi:10.1016/j.cmet.2013.10.002 (2013). [PubMed: 24206663]
46. Sallam Tet al.Feedback modulation of cholesterol metabolism by the lipid-responsive non-coding RNA LeXis. Nature534, 124–128, doi:10.1038/nature17674 (2016). [PubMed: 27251289]
47. Zhang Let al.Inhibition of cholesterol biosynthesis through RNF145-dependent ubiquitination of SCAP. Elife6, doi:10.7554/eLife.28766 (2017).
48. Sallam Tet al.Transcriptional regulation of macrophage cholesterol efflux and atherogenesis by a long noncoding RNA. Nat Med24, 304–312, doi:10.1038/nm.4479 (2018). [PubMed: 29431742]
49. Zhang Zet al.Collaborative interactions of heterogenous ribonucleoproteins contribute to transcriptional regulation of sterol metabolism in mice. Nat Commun11, 984, doi:10.1038/s41467-020-14711-4 (2020). [PubMed: 32080181]
50. Dobin Aet al.STAR: ultrafast universal RNA-seq aligner. Bioinformatics29, 15–21, doi:10.1093/bioinformatics/bts635 (2013). [PubMed: 23104886]
51. Casero Det al.Long non-coding RNA profiling of human lymphoid progenitor cells reveals transcriptional divergence of B cell and T cell lineages. Nat Immunol, doi:10.1038/ni.3299 (2015).
52. Love MI, Huber W & Anders S Moderated estimation of fold change and dispersion for RNA-seq data with DESeq2. Genome Biol 15, 550, doi:10.1186/s13059-014-0550-8 (2014). [PubMed: 25516281]
53. Si Y, Liu P, Li P & Brutnell TP Model-based clustering for RNA-seq data. Bioinformatics, doi:10.1093/bioinformatics/btt632 (2013).

54. Zhou Yet al.Metascape provides a biologist-oriented resource for the analysis of systems-level datasets. Nat Commun10, 1523, doi:10.1038/s41467-019-09234-6 (2019). [PubMed: 30944313]

55. Dominissini Det al.Topology of the human and mouse m6A RNA methylomes revealed by m6A-seq. Nature485, 201–206, doi:10.1038/nature11112 (2012). [PubMed: 22575960]

56. Salmon-Divon M, Dvinge H, Tammoja K & Bertone P PeakAnalyzer: genome-wide annotation of chromatin binding and modification loci. BMC Bioinformatics 11, 415, doi:10.1186/1471-2105-11-415 (2010). [PubMed: 20691053]

57. Bailey TL & Machanick P Inferring direct DNA binding from ChIP-seq. Nucleic Acids Res 40, e128, doi:10.1093/nar/gks433 (2012). [PubMed: 22610855]

58. Rogers GWet al.High throughput microplate respiratory measurements using minimal quantities of isolated mitochondria. PLoS One6, e21746, doi:10.1371/journal.pone.0021746 (2011). [PubMed: 21799747]

59. Kedersha N & Anderson P Mammalian stress granules and processing bodies. Methods Enzymol 431, 61–81, doi:10.1016/S0076-6879(07)31005-7 (2007). [PubMed: 17923231]

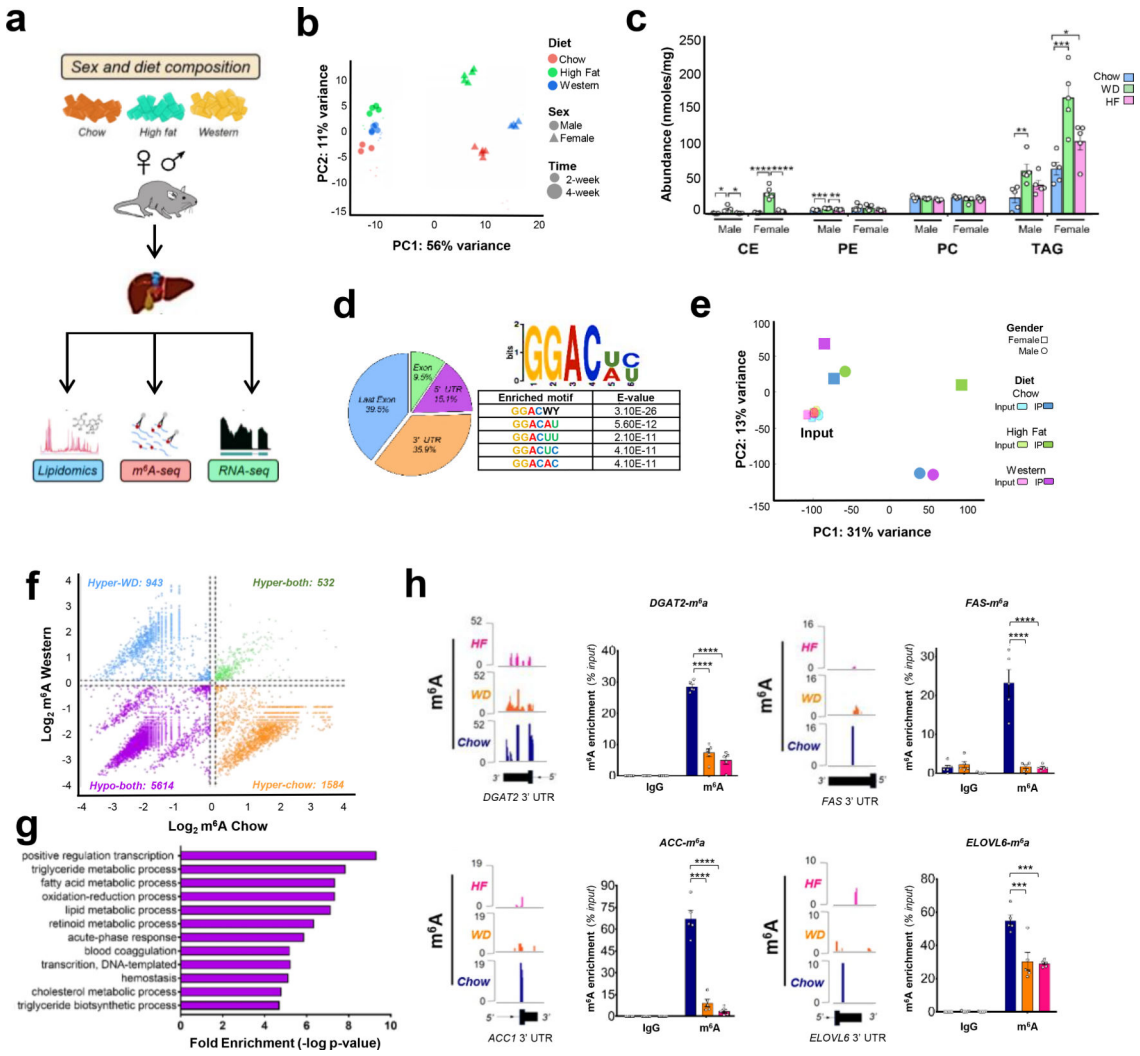

Fig. 1 |. RNA methylation strongly enriches lipogenic transcripts and is dynamically regulated with diet.

a, Schematic of experimental design. **b,** Principal component analysis (PCA) of gene expression for mouse liver samples under chow (n = 5 females, 3 males), WD (n = 4 females, 5 males), and HF diet (n = 5 females, 4 males). The first two components (PC1, PC2) are shown along with the percent of gene expression variance explained. Clustering was obtained with data from all detected genes without additional filters. HF=High Fat, WD=Western Diet. Results are representative of 2 independent experiments. **c,** Major hepatic lipid species analyzed by lipidomics in liver harvested from male and female mice fed chow, WD, or HF (n = 5 per group). Results are representative of 2 independent experiments. **d,** Pie chart illustrating relative position of m^{6}A on immunoprecipitated transcripts and motif enrichment analysis of m^{6}A-containing RNAs. E-values were computed as the enrichment p-value (Fisher's Exact Test for enrichment of the motif in the positive sequences) times the number of candidate motifs tested. **e,** PCA plot for m^{6}A-seq in mouse liver under different conditions. Both input and m^{6}A immunoprecipitated samples are displayed. **f,** Scatter plot comparing m^{6}A enrichment between chow and WD-fed male livers. Hyper-methylated peaks with significantly higher m^{6}A enrichment ($\log_2$m^{6}A > 0)

in chow compared to WD are noted with orange dots, and hypo-methylated peaks with significantly lower m^6A enrichment ($log_2m^6A<0$) in chow compared to WD are noted with blue dots. Genes with no significant difference in m^6A enrichment between chow and WD are shown in orange (hypermethylated in chow compared to WD) and purple (hypomethylated in chow compared to WD). **g,** DAVID functional annotation of top 500 genes with highest m^6A enrichment in male mice fed chow versus WD diet. Gene ontology analysis was performed with –log10 (p value) plotted (x axis) as a function of classification meeting a p value of < 0.001. **h,** UCSC browser screenshots and enrichment of m^6A modification on lipogenic transcripts in male liver as determined by m^6A-IP-qPCR (n=5 per group). The relative enrichment of m^6A in each sample was calculated by normalizing to tenfold input. Results are representative of 2 independent experiments. All mice were fed the indicated diet for 4 weeks and fasted for 4 hrs prior to sacrifice. Values are mean ± s.e.m. of five biological replicates (**c,h**). *P* values were calculated using one-way analysis of variance (ANOVA) followed by a multi-group comparison test (Fisher's) in **c** and **h** or unpaired two-tailed t-test in **g.** **P<0.05; ** P<0.01; *** P<0.001; **** P<0.0001.* The precise *n, P* values, and details of the statistical testing are provided in the source data file.

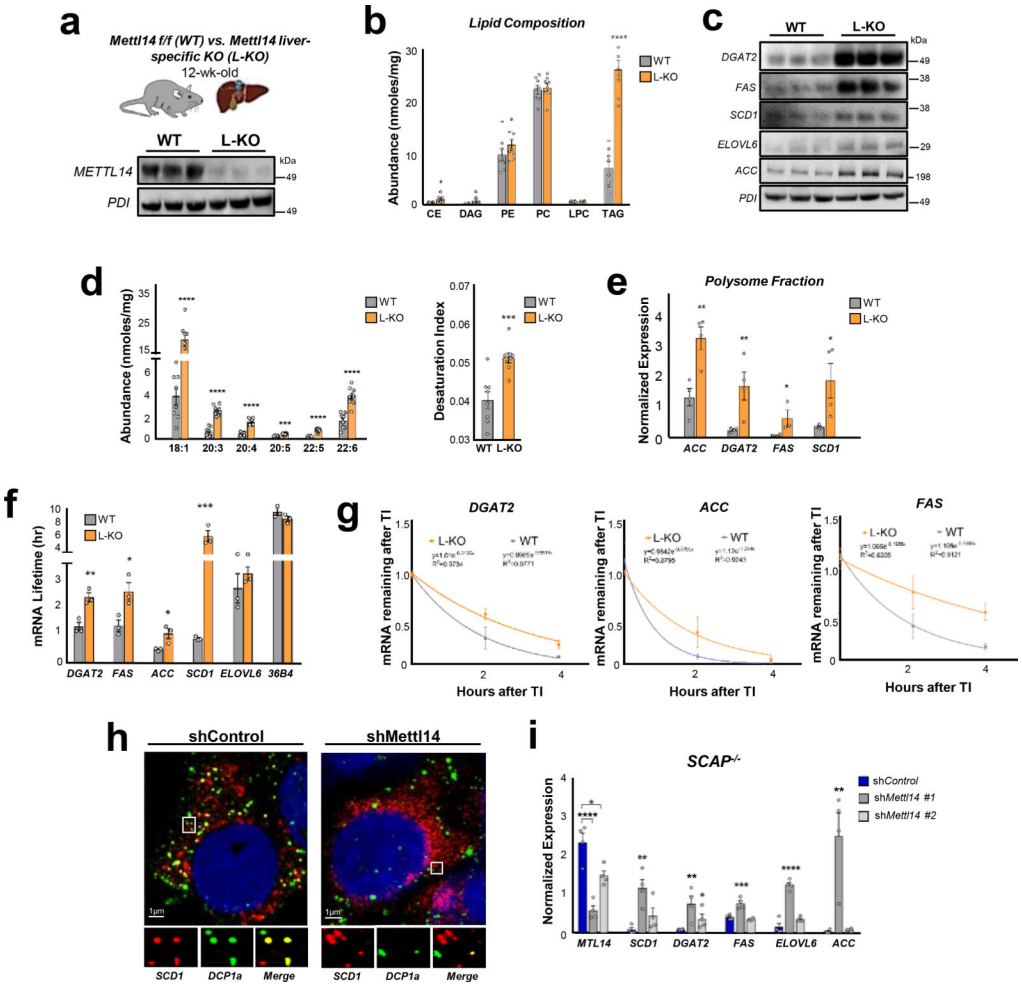

Fig. 2 |. Liver-specific deletion of the m^{6}A methylase METTL14 increases de-novo lipogenesis and hepatic triglyceride content.

a, Western blot from liver of WT and *Mettl14* L-KO chow-fed male mice. Equal amounts of protein were pooled from eight animals and run in triplicate. The experiment was repeated 3 times with similar results. **b,** Quantification of major lipid species detected in livers of chow-fed male WT and *Mettl14* L-KO mice by unbiased lipidomics (*n* = 8 per group). **c,** Western blot comparing lipogenic protein levels in WT versus *Mettl14* L-KO chow-fed male mice livers (*n* = 8 per group). Equal amounts of protein were pooled from eight animals per group and run in triplicate. The experiment was repeated 3 times with similar results. **d,** Unbiased lipidomic measurement from liver of PUFAs (measured by lipidomics) and *SCD1* index for WT and *Mettl14* L-KO chow-fed male mice (*n* = 8 per group). **e,** qPCR analysis of transcript levels in polysome fraction from WT and *Mettl14* L-KO chow-fed male livers (*n* = 4). The experiment was repeated 3 times with similar results. **f,** mRNA lifetime of lipogenic transcripts in primary hepatocytes harvested from livers of chow-fed WT and *Mettl14* L-KO mice (*n*=3). **g,** Quantification of transcript abundance by qPCR at 2hr and 4hr after transcription inhibition in primary hepatocytes harvested from WT and *Mettl14* L-KO chow-fed male livers (*n*=3). **h,** Single-molecule RNA FISH showing localization of *SCD1* mRNA in WT and *Mettl14* knockdown AML cells. Images are representative of

three independent experiments. **i,** qPCR analysis of lipogenic gene expression in *METTL14*-knockdown versus control in *SCAP*-KO HEK293 cells *(n*=4). The experiment was repeated 2 times with similar results. All mice were fed chow diet for the indicated time period and fasted for 4 hrs prior to sacrifice. Values are mean ± s.e.m. of 3(**f,g**), 4(**e,i**), or 8(**b,d**) independent biological replicates. *P* values were calculated using unpaired two-tailed *t*-test (**b,d,e,f,g,i**). ** P<0.05; ** P<0.01; *** P<0.001; **** P<0.0001.* The precise *n, P* values, and details of the statistical testing are provided in the source data file.

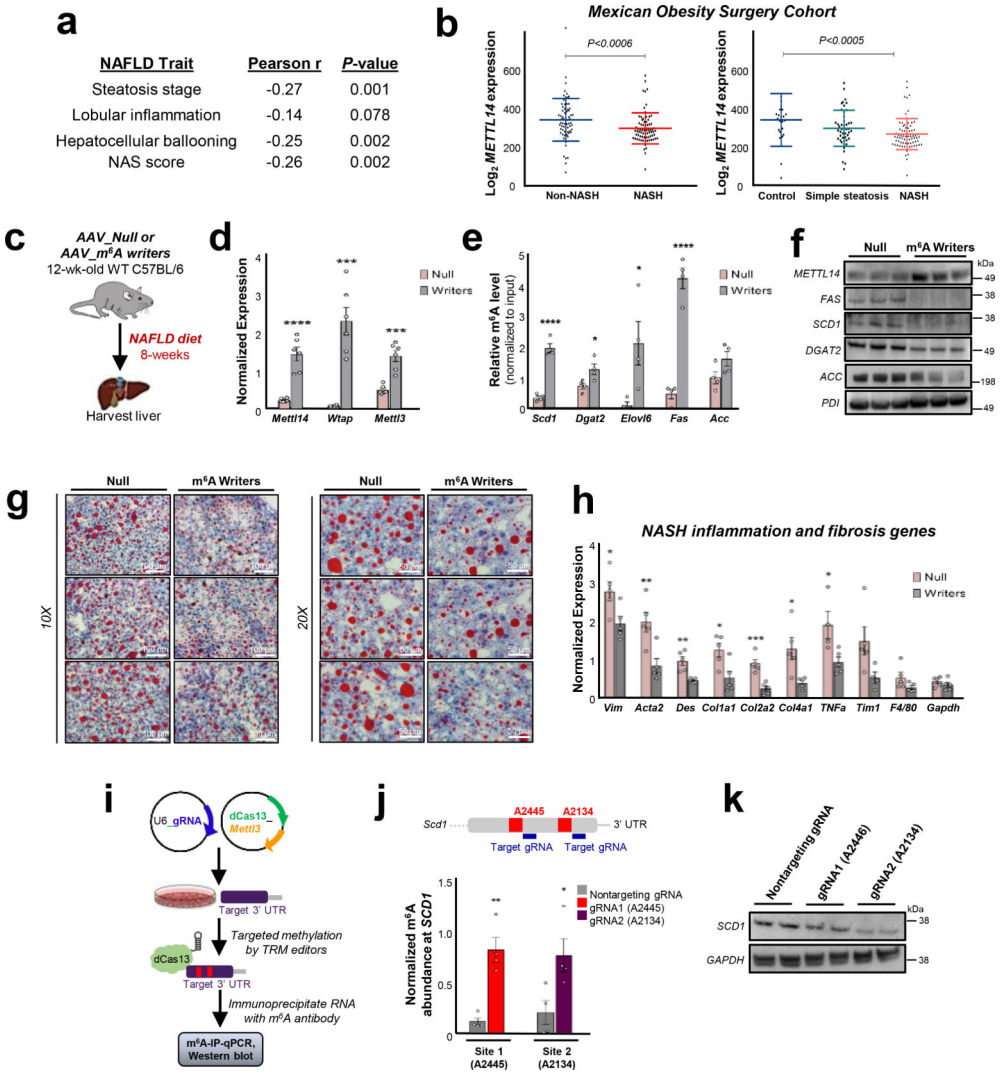

Fig. 3 |. METTL14 expression is inversely correlated with fatty liver disease and hepatic triglyceride content.

a, Pearson correlation coefficient and *P*-value comparing *METTL14* expression and NAFLD traits in humans (n=144) from Mexican Obesity Surgery (MOBES) Cohort. **b,** Correlation between *METTL14* expression and NAFLD from Mexican Obesity Surgery (MOBES) cohort. **c,** Schematic of gene therapy design. **d,** Gene expression in liver harvested from mice injected with AAV8.tbg.*Mettl14*, AAV8.tbg.*Mettl3 and* AAV8.tbg.*Wtap* 'writers' versus equal amount AAV8.tbg.null (n = 6). **e,** Quantification of m^{6}A abundance on lipogenic mRNAs as measured by m^{6}A-IP-qPCR from livers of mice injected with AAV8.tbg.*Mettl14*, AAV8.tbg.*Mettl3 and* AAV8.tbg.*Wtap* 'writers' versus equal amount AAV8.tbg.null (n = 4). The experiment was repeated two times with similar results. **f,** Western blot comparing lipogenic protein levels in livers of mice overexpressing m^{6}A writers compared to control. Equal amounts of protein were pooled from 6 animals per group and run in triplicate. The experiment was repeated three times with similar results. **g,** Oil-Red-O staining of frozen liver sections from mice in (**f**). Images are representative of three independent biological replicates. Scale bar equals 100 microns (left), 50 microns (right). **h**, qPCR

analysis of NASH-related fibrosis and inflammatory gene expression from livers of mice treated with AAV overexpression of m^6A writers or null ($n = 5$). The experiment was repeated two times with similar results. **i,** Schematic of *in-vitro* targeted RNA modification (TRM) editor experiment. **j,** Quantification of m^6A abundance at *Scd1* by m^6A-IP-qPCR following transfection of TRM editors ($n = 4$ independent biological replicates). Values were normalized to a non-targeted m^6A site located in the 3' UTR of *Scd1.* **k,** Western blot comparing *SCD1* protein levels in cells transfected with gRNAs targeting A2445 or A2134 versus cells transfected with nontargeting gRNA. Samples were pooled from 3 independent biological replicates and run in duplicate. The experiment was performed three times with similar results. All mice were fed NASH diet for 8 weeks and fasted for 4 hrs prior to sacrifice. Values are mean ± s.e.m. of 4 (**e,j**), 5 (**h**), or 6 (**d**) biological replicates. *P* values were calculated using one-way analysis of variance (ANOVA) followed by multi-group comparison (Fisher's) in **b** or unpaired two-tailed *t*-test (**b**,**d,e,h,j**) *$P<0.05$; **$P<0.01$; ***$P<0.001$; ****$P<0.0001$. The precise *n, P* values, and details of the statistical testing are provided in the source data file.

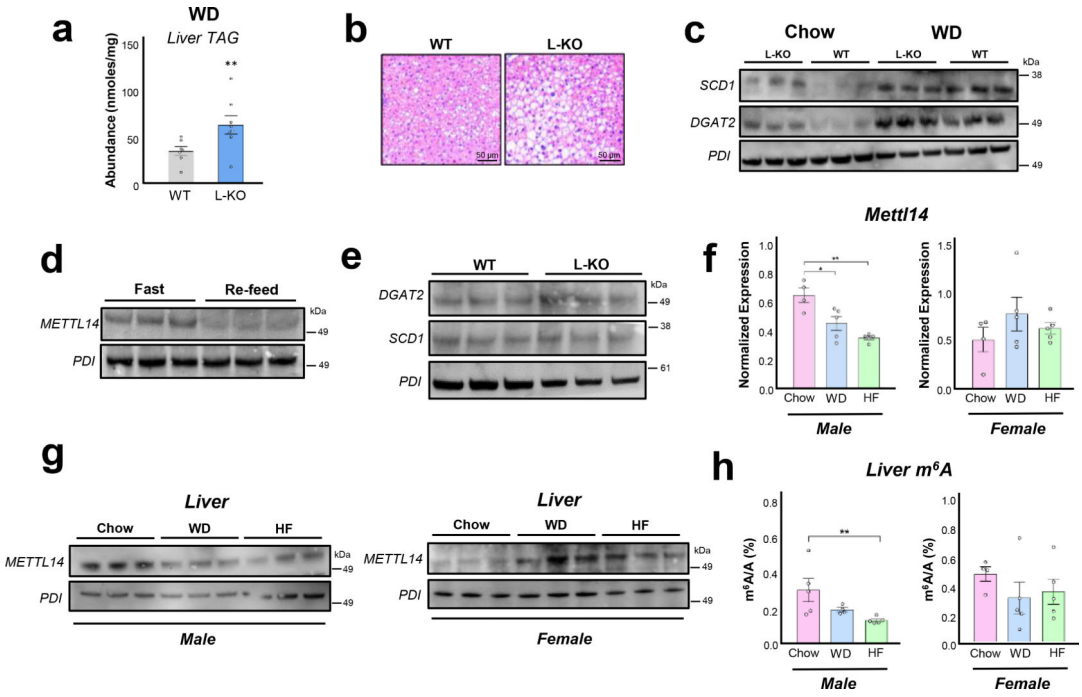

Fig. 4 |. m^{6}A machinery is dynamically regulated by diet and exhibits sexual dimorphism.
a, Hepatic TAG content determined by lipidomics from WT and *Mettl14* L-KO mice under WD feeding (n = 7 WT mice, n = 8 KO mice). **b,** H&E staining of representative livers from male WD-fed WT or *Mettl14* L-KO mice. Images are representative of three independent biological replicates. **c,** Western blot comparing lipogenic protein levels in WT and *Mettl14* L-KO livers from chow and WD-fed male mice. Equal amounts of protein were pooled from five animals per group and run in triplicate. The experiment was repeated three times with similar results. **d,** Western blot showing *Mettl14* protein levels in liver of fasted (4 hr prior to sacrifice) versus re-fed (fasted overnight then re-fed for 4 hr) male mice. Equal amounts of protein were pooled from five animals per group and run in triplicate. The experiment was repeated three times with similar results. **e,** Western blot showing lipogenic protein levels in livers of male WT and *Mettl14* L-KO re-fed mice (fasted overnight then re-fed for 4 hr). Equal amounts of protein were pooled from five animals per group and run in triplicate. The experiment was repeated three times with similar results. **f,** qPCR analysis of *Mettl14* expression in male and female livers under different diets (n=5). **g,** Western blot showing *Mettl14* protein levels in liver harvested from male and female mice fed different diets. Equal amounts of protein were pooled from five animals per group and run in triplicate. The experiment was repeated three times with similar results. **h,** LC-MS quantification of hepatic m^{6}A levels in male and female mice fed different diets (n=5). One male WD sample and one female chow sample were identified as outliers and formally excluded (Grubbs, alpha = 0.05). Mice were fed the indicated diet for 4 weeks and fasted 4-hrs prior to sacrifice except for mice in (**d,e**). Mice in (**d,e**) were fasted overnight and then re-fed for 4-hrs prior to sacrifice. Values are mean ± s.e.m. of 5 (**f,h**), 7 (**a**), or 8 (**a**) independent biological replicates. P values were calculated using unpaired two-tailed t-test (**a**) or one-way analysis of variance (ANOVA) followed by multi-group comparison

(Fisher's) in **f** and **h**. **P<0.05; ** P<0.01; *** P<0.001; **** P<0.0001.* The precise *n, P* values, and details of the statistical testing are provided in the source data file.

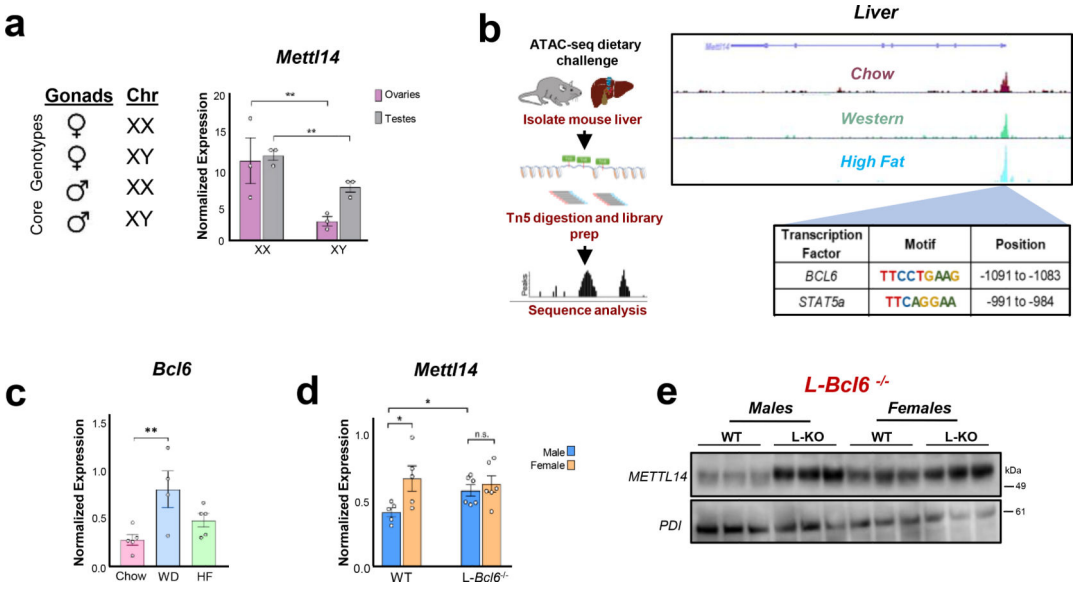

Fig. 5 |. m^{6}A machinery undergoes transcriptional regulation by sex-biased transcription factors. **a,** qPCR analysis of *Mettl14* expression in livers of male and female *Apoe*$^{-/-}$ mice (n=3) with core four genotypes. **b,** UCSC browser screenshot of ATAC-seq data for *Mettl14* promoter region from male mouse liver under different diets and transcription factor motifs identified at this site. Screenshots are representative of five independent biological replicates. **c,** qPCR analysis of *Bcl6* expression in male mouse livers under different diets (*n*=4 WD, *n*=5 chow, HF). The experiment was repeated three times with similar results. **d,** qPCR analysis of *Mettl14* expression in livers of male and female WD-fed WT and *Bcl6* L-KO mice (*n*=5 WT mice,6 *Bcl6* KO mice). The experiment was repeated three times with similar results. **e,** Western blot comparing *Mettl14* protein levels in livers of male and female WD-fed *Bcl6* KO mice compared to WD-fed WT mice. Equal amounts of protein were pooled from 5 animals per group and run in triplicate. The experiment was repeated two times with similar results. All mice were fed the indicated diet for 4 weeks and were fasted for 4-hrs prior to sacrifice. Values are mean ± s.e.m. of 3 (**a**), 4 (**c**), 5 (**c, d**), or 6 (**d**) independent biological replicates. *P* values were calculated using one-way analysis of variance (ANOVA) followed with multi-group comparison (Fisher's) in **c** or two-way ANOVA followed with multi-group comparison (Tukey) in **a** and **d.** **P<0.05; ** P<0.01; *** P<0.001; **** P<0.0001.* The precise *n, P* values, and details of the statistical testing are provided in the source data file.

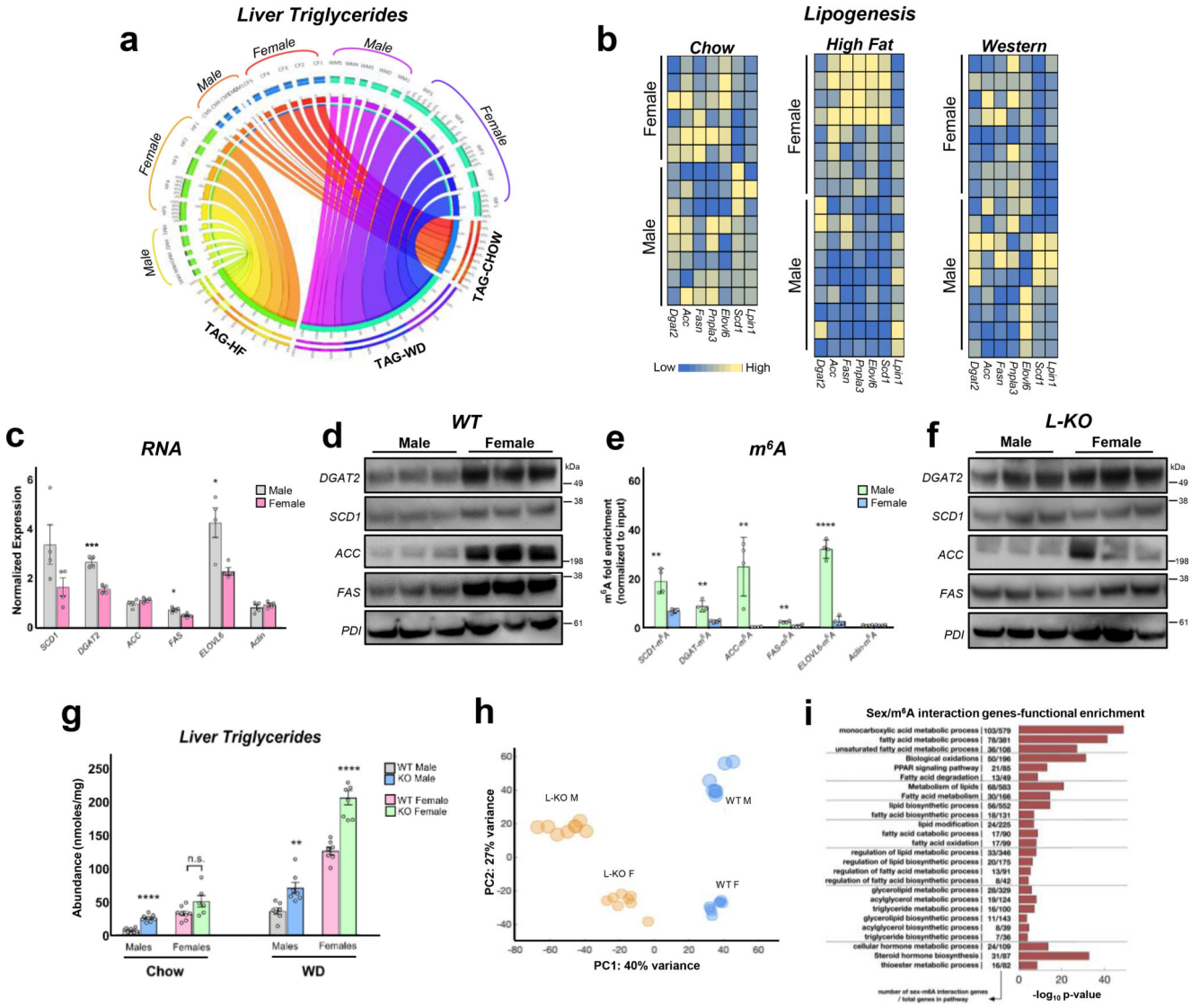

Fig. 6 |. Loss of m^{6}A significantly diminishes sex-specific differences in hepatic lipid composition.

a, CIRCOS plot of hepatic lipid content under different diets *(n*=5 per group). Width of connection indicates higher TAG content. **b,** Heatmap of lipogenic gene expression in livers of male and female mice under different diets *(n*=5 per group) based on RNA-seq. **c,** qPCR analysis of lipogenic gene expression in livers of WD-fed male and female mice *(n*=4 per group). The experiment was repeated three times with similar results. **d,** Western blots comparing lipogenic protein levels in WD-fed WT male and female liver. Equal amounts of protein were pooled from eight animals per group and run in triplicate. The experiment was repeated three times with similar results. **e,** m^{6}A-IP-qPCR validation of m^{6}A enrichment on lipogenic genes in livers of male and female mice *(n*=4 per group). The experiment was repeated two times with similar results. **f,** Western blots comparing lipogenic protein levels in WD-fed *Mettl14* L-KO male and female liver. Equal amounts of protein were pooled from eight animals per group and run in triplicate. The experiment was repeated three times with similar results. **g,** Quantification of hepatic TG content by

lipidomics in WT and *Mettl14* L-KO male and female livers *(n* = 6 KO chow-fed females, *n* = 7 WT and KO WD-fed males and females, *n* = 8 WT and KO chow-fed males and KO chow-fed females. **h,** Principal component analysis (PCA) of gene expression for male and female mouse livers in control and *Mettl14* L-KO samples (*n* = 7 WT males, *n* = 8 all other groups). Clustering was obtained with data from all detected genes without additional filters. **i,** Barplot of functional enrichment adjusted *P*-values (hypergeometric *P*-values after Benjamini-Hochberg correction) for genes significantly associated with sex-specific responses to *Mettl14*-L-KO (interaction genes). Ontology terms are grouped by gene member similarity. All mice were fed the indicated diet for 4 weeks and fasted for 4-hrs prior to sacrifice. Values are mean ± s.e.m. of 4 (**c,e**) or 6–8 (**g**) independent biological replicates. *P* values were calculated using unpaired two-tailed *t*-test (**c,e,g**). **P<0.05; ** P<0.01; *** P<0.001; **** P<0.0001.* The precise *n, P* values, and details of the statistical testing are provided in the source data file.